The "Year" of Tropical Convection (May 2008 to April 2010): Climate Variability and Weather Highlights

Duane E. Waliser[1], *Mitch Moncrieff*[2], *David Burrridge*[3], *Andreas H. Fink*[4], *Dave Gochis*[2], *B. N. Goswami*[2], *Bin Guan*[1], *Patrick Harr*[6], *Julian Heming*[7], *Huang-Hsuing Hsu*[8], *Christian Jakob*[9], *Matt Janiga*[10], *Richard Johnson*[11], *Sarah Jones*[12], *Peter Knippertz*[13], *Jose Marengo*[14], *Hanh Nguyen*[10], *Mick Pope*[9], *Yolande Serra*[15], *Chris Thorncroft*[10], *Matthew Wheeler*[16], *Robert Wood*[17], *Sandra Yuter*[18]

[1]*Jet Propulsion Laboratory, California Institute of Technology, Pasadena, CA, USA*
[2]*National Center for Atmospheric Research, Boulder, CO, USA*
[3]*THORPEX International Programme Office, World Meteorological Office, Geneva, Switzerland*
[4]*der Universitaet zu Koeln, Koeln, Germany*
[5]*Indian Institute of Tropical Meteorology, Pune, India*
[6]*Naval Postgraduate School, Monterey, CA, USA*
[7]*United Kingdom Meteorological Office, Exeter, England*
[8]*National Taiwan University, Taipei, Taiwan*
[9]*Melbourne University, Melbourne, Australia*
[10]*State University of New York, Albany, NY, USA*
[11]*Colorado State University, Fort Collins, CO, USA*
[12] *Karlsruhe Institute of Technology, Karlsruhe, Germany*
[13]*University of Leeds, Leeds, England*
[14]*Centro de Previsão de Tempo e Estudos Climáticos, Sao Paulo, Brazil*
[15]*University of Arizona, Tucson, AZ, USA*
[16]*Centre for Australian Weather and Climate Research, Melbourne, Australia*
[17]*University of Washington, Seattle, USA*
[18]*North Caroline State University, Raleigh, NC, USA*

Submitted to the

Bulletin of the American Meteorological Society

November 2010

Corresponding author: *Duane Waliser, duane.waliser@jpl.nasa.gov, Jet Propulsion Laboratory, MS 183-505, California Institute of Technology, 4800 Oak Grove Drive, Pasadena, CA 91109*

Abstract

The representation of tropical convection remains a serious challenge to the skillfulness of our weather and climate prediction systems. To address this challenge, the World Climate Research Program (WCRP) and World Weather Research Program (WWRP)/THORPEX are conducting a joint research activity consisting of a focus period approach along with an integrated research framework tailored to exploit the vast amounts of existing observations, expanding computational resources and the development of new, high-resolution modeling frameworks. The objective of the Year of Tropical Convection (YOTC) is to use these constructs to advance the characterization, modeling, parameterization and prediction of multi-scale tropical convection, including relevant two-way interactions between tropical and extra-tropical systems. This article highlights the diverse array of scientifically interesting and socially important weather and climate events associated with the WCRP-WWRP/THORPEX YOTC period of interest: May 2008 to April 2010. Notable during this two-year period was the change from cool to warm ENSO states and the associated modulation of a wide range of smaller time and space scale tropical convection features. This period included a near record-setting wet N. American monsoon in 2008 and a very severe monsoon drought in India in 2009. There was also a plethora of tropical wave activity including easterly waves, the Madden-Julian Oscillation and convectively-coupled equatorial wave interactions. Numerous cases of high impact rainfall events occurred along with notable features in the tropical cyclone record. The intent of this article is to highlight these features and phenomena, and in turn promote their interrogation via theory, observations and models in concert with the YOTC program so that improved understanding and predictions of tropical convection can be afforded.

1 Introduction

The realistic representation of tropical convection in our global atmospheric models is a long-standing grand challenge for numerical weather forecasts and global climate predictions (see companion article Moncrieff et al. 2010; hereafter M10). Our lack of fundamental knowledge and practical capabilities in this area leaves us disadvantaged in simulating and/or predicting prominent phenomena of the tropical atmosphere such as the Intertropical Convergence Zone (ITCZ), El Nino – Southern Oscillation (ENSO), monsoons and their active/break periods, the Madden-Julian Oscillation (MJO), easterly waves and tropical cyclones, subtropical stratus decks, and even the diurnal cycle. Furthermore, tropical climate and weather disturbances strongly influence stratospheric-tropospheric exchange and the extra-tropics. To address this challenge, the World Climate Research Program (WCRP) and World Weather Research Program (WWRP)/THORPEX jointly proposed and are implementing a coordinated research program involving observing, modeling and forecasting of organized tropical convection – referred to as the "Year of Tropical Convection" (see www.ucar.edu/yotc). A key component of the motivation of YOTC is that there have been substantial investments in the Earth Science infrastructure over the previous decades. These are now realized in terms of a comprehensive satellite observing system (e.g., Earth Observing System), operational buoy arrays in each of the tropical oceans, global analyses and forecast systems that are now carried out at resolutions less than 25km, and a number of global, high-resolution, convection-permitting modeling systems. Based on these investments, including field programs already in place, a key precept of YOTC is that a tractable and promising research program can be constructed from the presently available resources, through a focus period approach, in much the same way field programs and specific phenomenological cases focus and magnify the community's attention and efforts (e.g., First Global GARP Experiment (FGGE), TOGA COARE).

The YOTC period is May 2008 to April 2010; its choice developed from deliberations that started with the activity's conception at a WCRP-THORPEX sponsored meeting in 2006 [*Moncrieff et al.*, 2007], its subsequent Science Planning meeting in 2007 [*Waliser and Moncrieff*, 2008], and the YOTC Implementation Planning (IP) meeting in 2009 (see Implementation Plan at www.ucar.edu/yotc). While the target period was initially designed to be a year, its extension to a full two years was proposed and agreed to at the IP meeting in concert with the realization that a second year would allow YOTC to capture a period of both La Nina and El Nino conditions (see Figure 1). In this article, we describe this period in terms of its anomalous low-frequency characteristics as well as highlight the most interesting and impactful synoptic features. The description of the latter is largely aligned with the targeted phenomenological areas outlined in the YOTC Science Plan. These include: 1) the Madden-Julian Oscillation (MJO) and other convectively-coupled equatorial waves (CCEWs), 2) easterly waves and tropical cyclones (TCs), 3) monsoons, 4) tropical-extratropical interactions, and 5) the diurnal cycle. The objective of this overview article is to set the stage for more targeted and in depth observation, modeling and prediction studies for the YOTC period, following the strategies outlined in the YOTC IP. Following the descriptions of the low-frequency and synoptic characteristics is a Summary and Discussion section that highlights the more notable features of the period. It concludes with an overview of YOTC's plans to leverage these features and events for case-study research to improve our understanding, modeling and prediction capabilities associated with tropical convection.

2 Background Conditions and Low-Frequency Variability

Some elements of weather and higher frequency climate variability that are targeted by YOTC depend on characteristics of the conditions set up by lower-frequency variability. For example, the spatial characteristics and manifestations of intraseasonal variability (ISV; e.g., MJO) can be modified by the conditions of ENSO and the Indian Ocean Dipole (IOD) [e.g., *Hendon et al.*, 1999; *Kessler*, 2001; *Waliser et al.*, 2001; *Lau*, 2005; *Hendon et al.*, 2007; *Rao et al.*, 2007; *Ajayamohan et al.*, 2009]. Moreover, these low-frequency tropical conditions influence the manifestations of extra-tropical patterns of variability (e.g., Pacific North America (PNA)) [e.g., Horel and Wallace, 1982; Renwick and Wallace, 1996; Kumar and Hoerling, 1998; Newman and Sardeshmukh, 1998; Wallace, 2000; Ambaum et al., 2001; Giannini et al., 2001; Hastenrath and Greischar, 2001; Ostermeier and Wallace, 2003]. For these reasons, we begin by documenting the background conditions and evolution of low-frequency climate patterns, including extra-tropical modes of variability. Figure 1 shows the anomalous characteristics of SST in the three tropical ocean basins during the YOTC period[1]. Starting with the Pacific, the early half the YOTC period is characterized by modest La Nina conditions while the latter half is characterized by modest El Nino conditions. Closer examination shows that the 2008-09 boreal winter period is cool and the 2009-10 boreal winter period is warm, both spring-to-summer periods tend to exhibit warming conditions, and the 2008 (2009) boreal fall undergoes cooling (warming) conditions. Overall the largest and longer-lived anomalous conditions tend to be more strongly exhibited in Nino 4 compared to Nino 3. This contrast in anomalous SST (i.e. La Nina vs El Nino) between the first and second half of the YOTC period represents an excellent contrast for studying its effects on tropical convection characteristics.

For the Indian Ocean, there is some similarity to the Pacific, with a tendency towards cool (warm) conditions in the first (second) half of the YOTC period, albeit with about half or less the amplitudes exhibited in the Pacific. Subtracting the eastern Indian Ocean time series from the western gives the IOD Mode Index [DMI, not shown, *Saji et al.*, 1999]. The DMI index is an indicator of the east-west temperature gradient across the tropical Indian Ocean, linked to the Indian Ocean Dipole or Zonal Mode. Extreme September-October-November rainfall in tropical East Africa has been associated with periods of persistently high DMI [*Black et al.*, 2003]. During most of YOTC, the index generally was positive, with the summer of 2008 being a relatively short-lived, large-amplitude DMI event. Weak negative values of the DMI occur during the winter of 2008-09 and to a lesser extent in fall of 2009 (not shown). For the Atlantic, the most remarkable feature is the exceptional warming that develops during the winter of 2009-10. This is a peak value when considering the record back to 1982. The southern Tropical Atlantic exhibits warm conditions over nearly all the YOTC period with peak magnitudes typical when considering the most recent three decades (not shown).

Figure 2 illustrates the evolution of four extra-tropical modes of variability during the YOTC period. These four extra-tropical modes include the PNA, Arctic Oscillation (AO), North Atlantic Oscillation (NAO), and the Antarctic Oscillation (AAO)[2]. The NAO and AO exhibit an overall anti-correlation with the Nino4 and northern Tropical Atlantic indices shown in Figure 1, with each being in mostly a positive (negative) phase during the Pacific cool (warm) period(s). The AAO exhibits a strong anti-correlation to the Nino4 index, while the PNA exhibits a strong correlation to the Nino3 index. Also illustrated in Figure 2 is the evolution of the Quasi-biennial Oscillation

42

[1] Nino 3 and Nino 4 are from www.cpc.noaa.gov/data/indices/, others are from ioc-goos-oopc.org/state_of_the_ocean/

[2] www.cpc.noaa.gov/data/indices/

(QBO) during YOTC, as indicated by the 50 hPa wind index time series. For the most part, the entire period of YOTC is dominated by a westerly phase of the QBO, with only the very ends of the period being relatively neutral. Finally, to comprehensively describe the background conditions under which the YOTC period evolved, it is worth noting that CO2 concentration averaged over the two year period was 386.8ppm[3], the solar cycle was largely in the minimum phase of the 11-year cycle[4], and there was no significant volcanic activity that occurred in or near the tropics.

3 Tropical Waves

3.1 Madden-Julian Oscillation

The MJO is of considerable interest in YOTC due to the considerable influence it has on other components of our weather and climate system, including monsoon onset and breaks, TCs, ENSO evolution, extra-tropical variability, etc. [*Madden and Julian*, 1971; *Lau and Waliser*, 2005; *Zhang*, 2005]. An overview of MJO-related tropical convective variability that occurred during the YOTC period is provided in Figure 3. This figure uses satellite outgoing longwave radiation (OLR) data filtered for eastward-propagating wavenumbers 1-5 and periods 30-96 days as a proxy for the convective variability associated with the MJO [*Wheeler and Kiladis*, 1999; *Wheeler and Weickmann*, 2001]. Six cases of relatively strong MJO activity have been identified during this period, labeled (a)-(f). By this measure, the three strongest cases of enhanced convection (i.e. negative OLR anomalies) associated with the MJO during YOTC were in April 2009 (case d), November 2009 (case e), and January 2010 (case f). These periods of MJO activity also show as being the strongest, although with different relative magnitudes, when viewed using the Realtime Multivariate MJO (RMM) index [*Wheeler and Hendon*, 2004], which includes lower and upper-tropospheric zonal winds in the MJO definition. Placing this activity into a historical context, the YOTC MJO cases were weaker than those that occurred in 8 of the previous 12 years, very much weaker than the MJO activity that occurred in the lead up to the 1997 El Nino, and a little weaker than the activity that occurred during TOGA COARE (not shown).

Highlighting the more notable cases, the *May-June 2008 (a)* event involved modulation of convective activity over much of the tropics, starting with the onset of the Indian monsoon over Kerala on 31st May 2008. Then, with propagation of the signal to the east Pacific by late June and early July, there was strong enhancement of convective activity of the east Pacific ITCZ, including the development of several tropical cyclones (TCs), including Boris, Cristina, Douglas, and Elida. The *April-May 2009 (d) event* included nearly 2 complete cycles of the MJO. The first exhibited strong interaction with other equatorial waves (see first case in Section 3.2) and has been implicated in the shift to El Niño conditions through the enhancement of westerly surface wind anomalies across the Pacific (once convection reached the Pacific in late April). The second cycle coincided with the Indian monsoon onset at Kerala on 23rd May. The *October-December 2009 (e)* event began with suppressed convection over the near-equatorial Indian Ocean in mid October, followed by a switch to enhanced convection over Africa and the western Indian Ocean which progressively gained in strength until peaking in the second week of November with the strongest negative OLR anomalies observed for the near-equatorial Indian Ocean for the whole of the YOTC period. Finally, for the *December 2009-February 2010 (f)* event, enhanced convection reached further eastward than any other MJO of the YOTC period, presumably helped by the warm Pacific conditions. The events discussed above, including the nuances of their initiation, propagation,

42

[3] ftp://ftp.cmdl.noaa.gov/ccg/co2/trends/co2_mm_mlo.txt
[4] http://www.swpc.noaa.gov/SolarCycle/

possible connections and their influences on TC formation make them excellent cases for forecast model verification studies.

3.2 Convectively Coupled Equatorial Waves

Here we focus on just two periods of notable occurrences of convectively-coupled equatorial waves (CCEWs) [*Kiladis et al.*, 2009]. The first was case involves multiple interacting waves during the period March-April 2009 (Figure 4; left). The MJO, (n=1) Equatorial Rossby (ER), and Kelvin waves were all simultaneously active, seemingly propagating through each other to account for the observed complex behavior of simultaneous eastward and westward propagation. For example, the enhanced convection that occurred near 90°E on 10th April appears to be a result of the superposition of the influence of all three waves propagating at different speeds and/or directions. The ER wave in this example originates from an earlier convective blow-up that occurred well to the east about 20 days previously. The Kelvin wave, on the other hand, originates from the Atlantic, crossing 0°E on about the 2nd April. A later strong Kelvin wave crossed the Atlantic and Africa in the first week of May.

The second case involves coherent westward movement of convection from east of the dateline in the Pacific to the Indian Ocean during the month of March 2010 (Figure 4; right). Consistent with the structure of an n=1 ER wave, this convection was mostly symmetric about the equator and occurred in conjunction with cyclonic circulation cells on either side of the equator. Imbedded within these cyclonic circulation cells were several TCs: TCs Tomas and Ului in the southern hemisphere and TC Omais (Agaton) in the northern hemisphere. TC Ului followed a long westward track, from ~170°E on 10th March to ~150°E on 21st March. In addition, prominent Kelvin wave activity was also observed during this case period (green contours in Figure 4). These cases, and others like them, represent stringent tests for our global forecast models to properly represent and as yet little attention has been paid to the verification of CCEW activity nor the metrics used for the evaluation (see M10).

3.3 Easterly Waves

As with the waves discussed above, easterly waves (EWs) play a key role in modulating tropical cyclogenesis, and are most prevalent during the NH summer over West Africa and the tropical Atlantic [*Kiladis et al.*, 2006] as well as the East Pacific [*Serra et al.*, 2008]. Figure 5 shows the July-September (JAS) variance of TRMM 3B42 precipitation rate [Huffman et al., 2007] in the "tropical depression" (TD) wavenumber frequency band (wavenumber -20 to -6 and period 2 to 5 days). Note that tropical cyclones may contribute to the TD-band variance, especially in the western Atlantic and Pacific north of 15°N. The top panel is indicative of climatological EW storm tracks [*Thorncroft and Hodges*, 2001]. The middle panel shows that 2008 was characterized by anomalously high TD variance in the West African and tropical Atlantic region. The region of maximum TD variance (6-15°N, 50°W-15°E) was 13% higher in 2008 than climatology. In contrast, TD variance in 2009 was 5% lower than climatology over the same region (Figure 5c). In 2008, TD variance was 20% below the 1998-2009 mean over the region 6-15°N, 150-80°W. Anomalously low TD variance was especially prominent in the Central Pacific consistent with the negative SST anomalies there (see Section 2). On the other hand, TD variance was 28% above climatology in 2009 over the same region consistent with the presence of above average SSTs. Similarly, west Pacific TD-band variance was also enhanced in 2009 [Hsu et al., 2009]. The relationship between the contrasting EW activity in 2008 and 2009, ENSO, and ISV associated with the MJO and CCWs is an area of research that could benefit from the YOTC.

Figure 6 provides a more detailed look at the tracks and characteristics of easterly waves during JAS 2008 and 2009. The Hovmöeller diagrams include precipitation rate and objectively determined EW tracks based on 700 hPa vorticity maxima [*Janiga*, 2010]. The period between mid-July and early September 2008 was associated with numerous intense African EWs moving over tropical North Africa into the East Atlantic. Consistent with past EW composite studies [see *Kiladis et al.*, 2006, and references therein] the peak precipitation rate is located ahead of the EW tracks or in the northerlies over Africa (Figure 6). A closer examination of the most intense waves reveals that mesoscale convective systems formed northwest of the mid-level trough and then moved southwestward but remained fairly coupled to the wave. One example of this is an EW that moved from the Ethiopian Highlands to the East Atlantic between July 14th and July 22nd, 2008 (see dashed box in Figure 6a). Both this wave and the preceding wave contributed to heavy rainfall and flooding in West Africa with rainfall totals between July 17th and the 21st in excess of 4 cm over much of West Africa and rainfall totals exceeding 10 cm in Burkina Faso and Liberia. Another high impact event occurred on Sep. 1, 2009 (see dashed box in Figure 6b) when an MCS, tightly coupled to the mid-level trough of an EW, produced 263 mm of rainfall in Ouagadougou, Burkina Faso according to rain gauges (not shown). Examinations of the relationship between sub-synoptic aspects of the structure of the EWs and these convective systems would be greatly aided by the high resolution of the YOTC analyses.

4 Tropical Cyclones

Tropical cyclones are by far one of the most significant manifestations of organized tropical convection, notably because of their sheer elegance as a physical system but also because of the societal need for ever-increasing accurate predictions of their strength and track. The tracks of all tropical cyclones during the YOTC period are illustrated in Figure 7, with those mentioned below annotated with a number at the start and end of the track. In 2008, the western North Pacific had 25 tropical storms with 12 becoming typhoons - a season with slightly below normal activity. Typhoon Jangmi (Figure 7a – track1) was the strongest tropical cyclone of the season across the whole northern hemisphere with sustained winds of 145 knots. Unusually, Japan received no direct landfalls during this season. The eastern North Pacific exhibited activity close to normal. Hurricane Norbert (Figure 7a – track 2) was the strongest of the season and was also one of three (with Julio and Lowell) to make landfall over Mexico. The North Atlantic was active; for the first time, major hurricanes (winds 100 knots or more) occurred in each of the five consecutive months from July to November. Hurricanes Fay, Gustav, Ike and Paloma all hit Cuba. Ike (Figure 7a– track 3) was one of the largest storms (in aerial size) ever recorded in this basin and caused a storm surge of up to 7m along the Gulf coast. In the North Indian Ocean, the most significant storm was Cyclone Nargis (Figure 7a – track 4), which made landfall over Myanmar and caused a huge storm surge up the Irrawaddy delta. This resulted in the loss of as many as 100,000 lives. During the 2008-9 southern hemisphere season four storms brought heavy rainfall to Madagascar. Cyclones Dominic and Ellie (Figure 7b – tracks 1 and 2) made landfall over the Australian coast whilst the strongest storm of the season, Hamish (Figure 7b – track 3) kept just offshore of the Australian east coast.

During the 2009 northern hemisphere season the El Niño induced stronger typhoons in the western North pacific and the storm tracks tended to originate further east into the central parts of the Pacific Ocean. The strongest typhoon of the season, Nida (Figure 7a – track 5), peaked with sustained winds of near 160 knots. Notable events were Typhoon Ketsana (Figure 7a – track 6) that caused extensive flooding in the Philippine capital Manila and later across Vietnam and Cambodia and slow moving Typhoon Parma (Figure 7a– track 7) that dumped an estimated 1.8 m rain over the northern Philippines. The El Niño also resulted in higher than normal activity in the eastern and

central North Pacific. Hurricane Rick (Figure 7a – track 8) became the second strongest east Pacific hurricane on record, making made landfall over Mexico, as did Hurricane Jimena (Figure 7a– track 9). In the North Atlantic, the El Niño resulted in a quiet season for the Caribbean and US. The most unusual event of the season was high latitude Hurricane Grace (Figure 7a – track 10) that developed near the Azores and eventually tracked across the UK as an extra-tropical system. In the North Indian Ocean, tropical storm Aila (Figure 7a – track 11) caused a storm surge of up to 3m across Bangladesh that resulted in hundreds of fatalities in this region. The most notable events for the 2009-10 southern hemisphere season included tropical storm Hubert (Figure 7b – track 4) that caused significant disruption over Madagascar. While activity was quiet around Australia, several storms [Laurence, Magda, Olga and Paul (Figure 7b – tracks 5, 6, 7 and 8)] impacted coastal regions. Mick and Tomas (Figure 7b – tracks 9 and 10) both affected Fiji and Ului (Figure 7b – track 11) was the strongest South Pacific cyclone for five years. To round off the season, a highly unusual tropical storm in the South Atlantic developed in March 2010 and was named Anita by Brazilian meteorological organizations (not shown). It was the first such storm to develop in this region since Catarina in 2004, although unlike Catarina posed no threat to land.

Tropical cyclone research in YOTC benefits from the occurrence of the THORPEX-Pacific Asian Regional Campaign (T-PARC) and Tropical Cyclone Structure-2008 (TCS-08) field experiments that conducted multiple aircraft operations into Typhoons Nuri, Sinlaku, Hagupit, and Jangmi. The science objectives of these campaigns included increasing understanding of tropical cyclone formation, structure and intensity change, extratropical transition, and the value of targeted observations. In particular, analysis of aircraft observations are being conducted with reference to gridded YOTC analyses fields provided by the European Centre for Medium-Range Weather Forecasts (ECMWF).

5 Monsoons

The monsoons exhibit considerable breadth in terms of the phenomena and range of space and time scales associated with tropical convection. This includes seasonal and planetary-scale changes in the atmospheric and ocean circulations, a preponderance of tropical wave activity, modulations of TCs other synoptic scales, and diurnal variations. The monsoons represent highly integrating features of tropical convection, and remain an ominous forecast challenge from not only their onset, but for subsequent breaks and active periods, extreme events and seasonal totals. Here, we highlight some of the notable monsoon characteristics during the YOTC period.

5.1 Indian

The top panel of Figure 8 shows the evolution of the Indian monsoon in terms of the All India Rainfall (AIR). The 2008 monsoon was considered to be a "normal" monsoon, garnering 98% of long-term average rainfall. However, 2009 was one of the worst drought monsoons over the past century with AIR being 22% below long term average. While the large-scale, slowly varying forcing from ENSO might be expected to play some role, there is also evidence the influence of intraseasonal variability (ISV) had a strong influence on the seasonal mean monsoon. In terms of temporal evolution, the near-normal monsoon of 2008 had many active episodes and only one substantial break (~ 20 Aug) while the severe-drought monsoon of 2009 was characterized by three substantial breaks. The extraordinary drought of 2009 is consistent with some recent studies [*Joseph et al.*, 2009] indicating that long breaks are responsible for Indian monsoon droughts. While the 2008 onset was on 31 May, close to climatology, in 2009 it took place on 23 May, a week before the normal onset date. However, the onset of 2009 had the characteristics of a 'bogus' onset [*Flatau*

et al., 2001] and was followed by a long break of more than a month duration covering most of June and part of July.

While seasonal mean values of large scale indices of the Indian monsoon, namely the kinetic energy of the tropical easterly jet (TEJ) and kinetic energy of the low level jet (LLJ), are typically weak during El Nino years, they were both found to be stronger in 2008 and 2009 (not shown). This suggests that the failure in monsoon precipitation during 2009 is not likely due to a monsoon weakening driven by El Nino. On the other hand, there were significant differences in ISV between 2008 and 2009; these are highlighted by the upper-middle and lower-middle panels of Figure 8. The time-latitude diagram of OLR anomalies shows that while both 2008 and 2009 were characterized by northward propagating disturbances, the timing and strength of these at the latitudes of the Indian subcontinent exhibited 2 (3) periods of rainfall suppression and 3 (2) periods of enhancement for 2008 (2009) during the JJAS time period. Moreover, the regressed 10-90 day filtered OLR and winds at 850 hPa with respect to the ISV-filtered OLR over central India shows a more canonical monsoon ISV structure (i.e. northwest-southeast titled dipole) in 2008 than in 2009 [e.g., Goswami, 2005; Waliser 2006]. Notable features are the absence of the dipole structure of convection in 2009 and a weaker cross-equatorial flow, implying weaker coupling between convection and circulation. Determining how these variations in ISV between the two years arose, and more importantly developing the ability to forecast them at lead times of 2-3 weeks, is a crucial challenge for YOTC. In this particular case, it is likely that ocean-atmosphere interaction may have played a role as the weakened cross-equatorial and break monsoon flows led to weakening of the upwelling along the Somali coast and in the Arabian Sea. This may well have had a further deleterious impact on the subsequent flow and monsoon evolution by reducing the north-south SST gradient that helps to support the low-level monsoon circulation.

5.2 East Asian / Western North Pacific

As with the Indian monsoon, the JAS seasonal-mean low-level circulation and convective activity in the East Asian/Western North Pacific (EA/WNP) monsoon region were distinctly different between 2008 and 2009. During JAS 2008, the monsoon trough was weaker than normal and confined mostly in the South China Sea, while the ridge was unusually strong and occupied the whole western North Pacific (WNP) from the equator to 50ºN (Figure 9). As a result, the whole WNP was characterized by an anticyclonic anomaly, except in the region to the southeast of Japan, and a rainfall deficit for most of the tropical WNP. In contrast, the monsoon trough was stronger and extended further eastward than normal in JAS 2009, while the ridge shifted more northward than usual. The corresponding circulation was characterized by a cyclonic anomaly in the South China Sea and the Philippine Sea and anticyclonic anomaly in the extratropical WNP. Moreover in 2009, the tropical EA/WNP from the South China Sea to 150ºE was dominated by a westerly anomaly. As a result, rainfall was above normal for most of the WNP, and in particular in the tropics from the South China Sea all the way to the Dateline.

Percentile maps show how anomalous the rainfall and specific humidity were during YOTC. The 850-hPa specific humidity was generally above the 85th percentile in the WNP west of 140ºE, but lower than the 15th percentile east of 160ºE in the prevailing region of the unusually strong subtropical ridge. Extremely low rainfall (below the 10th percentile) was observed in the region between 5ºN-15ºN and east of 140ºE where the anticyclonic circulation and easterly anomaly prevailed. In JAS 2009, the high specific humidity region extended further eastward and occupied almost the whole tropical and subtropical EA/WNP region. While rainfall was above the 50th percentile throughout most of this region, it was generally not as extreme as in specific humidity, except in the central rainfall-abundant areas where it exceeded 90 percentile. Extremely low rainfall

was found east of Taiwan and south of Japan and in the subtropical WNP east of 160ºE, in all cases where the anticyclonic anomalies prevailed. Note that typically JAS rainfall in the WNP is largely contributed by tropical cyclones, and this appears to be the case for the rainfall and TC distributions in 2008 and 2008 (see Figure 7). The characteristics above emphasize the multi-scale nature of tropical convection and the interactions between synoptic and finer scale convection, the large-scale circulations (e.g, monsoons and CCEWs) and basin-scale climate (e.g., ENSO).

5.3 Australian

The YOTC period covers two wet seasons in Northern Australia (NA), which occur in austral summer. Figure 10 shows a daily time series of rainfall together with the climatological rainfall distribution at Darwin (blue line). Significant intraseasonal variability is exhibited, some of which may be attributed to the MJO (see Section 3.1). However, tropical cyclones also contributed significantly to Darwin rainfall, namely TC Billy (Dec 2008), TC Lawrence (Dec 2009) and ex-TC Paula (Mar 2010) (see Section 4; Figure 7), as did a monsoonal low during late February 2010 and long-lived continental squall lines during late October 2009.

Through the development of an objective technique to better characterize the state of the NA wet season on any given day, Pope et al. [2009] showed that it is important to consider the entire wet season rather than just the embedded shorter monsoon period. This is because a significant fraction of the rainfall occurs outside the traditionally defined monsoon period. The state analysis technique involved the identification of five wet-season regimes from daily radiosonde data at Darwin. Three of the regimes, termed Deep West, Moist East and Shallow West are typically associated with rainfall, where Deep West identifies the active phase of the monsoon and Moist East signifies monsoon build-up, break and retreat conditions. Two of the five regimes (East and Dry East) represent generally dry conditions. The wet season onset can be identified by the first significant consecutive days of the Moist East Regime and monsoon onset is related to the first occurrences of the Deep West regime. Likewise the retreat of the monsoon and the end of the wet season can be determined as the last days of the Deep West and Moist East regimes respectively. Figure 10 shows the daily identification of wet-season regimes as described above for the two NA wet seasons within YOTC. Also shown are the climatological monsoon onset and retreat days (vertical dashed lines) and the monsoon onset and retreat days for the two seasons (arrows).

Using the Moist East regime as an indicator, the 2008-09 wet season started in early November and lasted until mid March. In contrast, the 2009-10 wet season started in early December and lasted well into April. This is consistent with La Niña conditions in 2008-09, which promote an early wet-season onset [*Nicholls et al.*, 1982; *Drosdowsky*, 1996], while the slight El Niño in 2009-10 favored a later wet-season onset. Using the definitions above, the onset in 2008 and 2009 occurred on December 18, 2008 and December 15 2009, respectively, close to the mean onset date December 19 [*Pope et al.*, 2009]. The retreat of the monsoon occurred on February 17 2009 and March 5 2010, respectively. Hence, the 2008-09 monsoon season was relatively short, while the 2009-10 season was of more or less average length, and the wet season as whole lasted significantly longer than in 2009/10 than 2008/09.

5.4 N. American

By measures such as all-Mexico JJA total rainfall, as indicated by gauge data (not shown) and OLR the 2008 North American Monsoon (NAM) was the largest since 1941. Positive rainfall anomalies in gauge data (not shown) and OLR (Figure 11a) were exhibited in nearly all regions of Mexico and throughout much of the U.S.-Mexico border region. Weakening wintertime La Niña conditions (Figure 11c and Figure 1) in the central and western Pacific, and an extended wintertime

drought and warm surface temperatures over western Mexico and the Southwest U.S., helped initiate an early, robust onset to the NAM in mid-to-late June. Regional precipitation tracking indices developed as part of the NAM Forecast Forum [*Gochis et al.*, 2009] showed all regions experiencing significant, accumulating precipitation through July. Persistent diabatic heating from convective activity (inferred from OLR anomalies) and a northwestward shift in the NAM ridge (Figure 11e) during July and August supported sustained moisture advection from the Gulf of California, tropical Eastern Pacific and the Gulf of Mexico into the NAM region [*Higgins et al.*, 2004]. As mentioned in Section 4, land-falling and near shore tropical storms also made significant contributions to rainfall totals of the NAM during JAS 2008, owing to the favorable steering circulations [*Englehart and Douglas*, 2001; *Wang et al.*, 2008; *Serra*, 2009], to rainfall totals of the NAM during JAS. Note that favorable circulation pattern for sustaining NAM rainfall has been suggested to steer tropical storms into Mexico, the Southwestern U.S., Baja California and the Texas Gulf Coast. Thus for a year like 2008, both the large-scale circulation and episodic extremes contributed to the record rainfall totals.

In contrast to 2008, changes in Pacific sea surface temperatures towards moderate El Niño conditions appeared to have had a significant impact on the 2009 NAM (Figure 11d). While the onset of the 2009 NAM was over a week early compared to climatology, the overall monsoon circulation pattern and its associated rainfall deteriorated substantially by late July. Consequently, July and August OLR anomalies (Figure 11b) were mostly positive over the southwest U.S. and Mexico. A number of areas of Mexico experienced some of the worst seasonal drought in recent history. Similarly, parts of western Arizona and the broader regions of the lower Colorado River valley experienced rainfall totals approaching only 50% of normal. Previous studies have shown that El Niño can suppresses NAM rainfall, particularly over southern and eastern Mexico [*Higgins et al.*, 1998; *Castro et al.*, 2001; *Gochis et al.*, 2007; *Liebmann et al.*, 2008] by enhancing convection in the Eastern Pacific ITCZ and reducing the northward transport of moisture, contributing to a poorly developed monsoon ridge structure (Figure 11f) and a weakened overall monsoon circulation [*Cavazos and Hastenrath*, 1990; *Gochis et al.*, 2007]. Related to this was a less than normal occurrence of tropical storm landfall and near-shore activity in both eastern and western NAM regions during 2009 (Figure 7).

5.5 S. American

The South American monsoon (SAMS) region extends from Southern Amazonia and the upper Parana-Basin, with the peak rainy season during December-February, the onset phase between September-November and the demise occurring after May [*Vera et al.*, 2006; *Marengo. J. et al.*, 2010]. Figure 12a shows that for 2008, rainfall in the onset phase was below average over central-southern Brazil in the SAMS region and most of Argentina (deficit exceeding 200 mm) while above normal rainfall was detected over the northern Amazon Basin (typical of the prevailing La Niña conditions). Later in December 2008-February 2009 (Figure 12b), rainfall was below average over the SAMS region, with deficits greater than 270 mm from the climatology. Above average rainfall was observed over the northern Amazon Basin and Northeast Brazil, with excesses larger than 200 mm in those regions with respect to climatology [*Marengo et al.*, 2010]. During the decay phase (Figure 12c), well above-average rainfall was observed over northeastern Brazil and northern Amazonia. The immediate cause of the unusually heavy rains across these regions was associated with an anomalously warm Tropical south Atlantic Ocean and a southward position of the ITCZ, that usually moves northward in April, but stayed in place until May. Another factor contributing to the intense rainfall in Northeast Brazil during this season was the active Madden-

Julian Oscillation (MJO) (See Figure 3; Note active MJO in eastern hemisphere, wide latitude averaging cancels signal out in this diagram over S. America).

For the 2009-2010 monsoon season warm conditions prevailed in the tropical Pacific. For the SAMS core region, rainfall in 2009 was near average, while dryer conditions persisted from northern Amazonia to Venezuela, due to an anomalously northward displacement of the ITCZ generated by warm surface waters in the tropical North Atlantic. During the peak season Figure 12e), rainfall totals were near average over the southern Amazon basin, and slightly below average over central Brazil and the north-central Amazon basin (deficits of about 50-100 mm). Above-average rainfall was observed over southern South America while below average rainfall was observed over most of eastern Brazil. During March and April (Figure 12f), rainfall totals are below average over central Brazil and Northeast Brazil, with deficits of about 50-100 mm. Near-average rainfall totals were observed over southeastern Brazil, while above-average rainfall totals were observed over southern Northeast Brazil in the decay phase.

5.6 African

The year-to-year variability of Sahel rainfall, and thus the west African monsoon, is of great interest due to the very strong north-south gradient in natural and anthropogenic conditions. Figure 13 shows that both 2008 and 2009 May-September seasons were slightly wetter than the long-term average, consistent with a recent wet trend in this region [*Fink et al.*, 2010]. Further scrutiny illustrates that the anomalously wet Sahel signal in both years was mainly exhibited in the western Sahel west of about 0^{o}E. The wet West Sahel in 2008 was part of a regional-scale wet anomaly that covered most of the West African region down to the Guinea Coast. Other notable anomalies in 2008 included a drier (wetter) than normal Sudan (Ethiopian highlands). While the West Sahel was also wet in 2009, the West African region as a whole was drier compared to climatology, with notable dry anomalies in Liberia and the Ivory Coast, in much of Nigeria, and most prominently (compared to 2008) in the Sudan and Chad regions. The more widespread dry anomalies seen in 2009 compared to 2008 are consistent with the developing El Nino (Figure 1). In addition, the relatively dry Guinea Coast and wet Sahel would classify the 2009 season as a "dipole year" [*Ward*, 1998], which is consistent with the observed cooler equatorial Atlantic during summer 2009 compared to 2008 (Figure 1)

6 Tropical – Extratropical Interactions

6.1 Extratropical transition of tropical cyclones

During extratropical transition (ET), tropical cyclones undergo significant structural changes, especially with regards to the distribution of deep convection, clouds and precipitation [*Jones et al.*, 2003]. The interaction with the midlatitude flow during ET can lead to the excitation of a Rossby wavetrain [*Harr and Dea*, 2009] and thus impact the midlatitude weather and predictability far from the location of the ET event [*Anwender et al.*, 2008; *Harr et al.*, 2008] (see also M10). A primary objective of the THORPEX Pacific Asian Regional Campaign (T-PARC), that took place during the YOTC period, was to increase understanding of the impact of tropical cyclone structure on the ET process and subsequent midlatitude downstream development.

A unique set of observations of the structural changes during the ET of Typhoon Sinlaku (2008) was obtained during T-PARC. Following recurvature, Sinlaku was significantly altered by strong vertical wind shear from the west. The vortex core was tilted toward the east and the low-level circulation center was fully exposed as deep convection was suppressed. As the decaying Sinlaku approached southern Japan, several episodes of deep convection erupted to the east and

downshear of the circulation center. The tropical cyclone re-intensified to typhoon strength with a circulation center co-located with new episodes of the deep convection. *In situ* measurements obtained by T-PARC documented how the characteristic monopole vorticity structure evolved to a low-level center associated with the original tropical cyclone and a new vorticity center to the northeast, located in the region of the episodes of deep convection. Analysis of convective and stratiform precipitation from YOTC ECMWF analyses defined the presence of both cloud types in the region of the new vorticity maximum. Therefore, the diabatic fields indicate a tropical mesoscale circulation system with a stratiform region downstream from a leading convective cell. The re-intensification period resulted in a stronger intensity and modified structure of Sinlaku as it eventually underwent ET, and thus had an impact on its interaction with the midlatitude flow. During and following the ET a small-scale Rossby wavetrain developed and appeared to interact with a larger-scale midlatitude Rossby wavetrain (Figure 14c) No Rossby wavetrain is seen downstream of the second T-PARC ET case, Typhoon Jangmi. However, the divergent outflow from Jangmi appeared to accelerate a midlatitude jet streak.

During the YOTC period, low predictability, identified as increased standard deviation in the 3, 5 and 7 day forecasts of the ECMWF ensemble prediction system (EPS), is particularly marked when a clearly defined Rossby wavetrain develops or amplifies directly downstream of an ET event. This is seen for the ET of Halong in May 2008 (Figure 14a,b), Bavi in October 2008 (Figure 14c) and a further seven examples in the western North Pacific, two in the North Atlantic and three in the Southern Hemisphere. In contrast, following the ET of Rammasun (Figure 14a,b), ridging occurs downstream of the ET but the Rossby wavetrain does not amplify until it reaches the eastern North Pacific. The EPS spread also increases at this stage. Similar behavior was seen in two other cases during the YOTC period. For Nakri in 2008 (Figure 14a,b) and five Southern Hemisphere ETs, the main signal is a midlatitude Rossby wavetrain that is not modified during ET and exhibits weak to moderate EPS spread.

The YOTC period offers cases both of structural changes during ET as well as a variety of interactions between ET systems and the midlatitude flow. A priority for research with the combination of YOTC data sets and T-PARC observations will be to quantify the role of structural changes of the tropical cyclone before and during ET (e.g., increased outflow at upper levels, increased heat and moisture transport to midlatitudes) on the downstream midlatitude predictability (see M10).

6.2 Extratropical Influences on the Tropics

Upper-level disturbances penetrating from the extratropics into the subtropics and outer tropics can significantly influence the weather in the tropical belt [*Knippertz*, 2007 and references therein]. The eastern tropical Atlantic and Pacific Oceans and the adjacent landmasses are frequently affected by such tropical–extratropical interactions. In West Africa, upper-level disturbances regularly trigger moderate precipitation events during the boreal-winter dry season [*Knippertz and Fink*, 2008; 2009]. These significant anomalies can lead to high impacts on the affected population (e.g., rotting harvests, improved Mango yield and grazing conditions, locusts). In extreme cases, heavy precipitation, flooding, destruction of infrastructure, and loss of lives can occur [*Knippertz and Martin*, 2005; *Meier and Knippertz*, 2009].

During the two dry seasons of the YOTC period five significant West African wet episodes occurred: 05–06 December 2008, 08–09 January 2009, 16–19 February 2009, 31 October–01 November 2009, and 12–14 December 2009. Here we will briefly discuss the February 2009 case as an illustration of the phenomenon [*Knippertz and Fink*, 2008; 2009]. Figure 15a shows accumulated precipitation from over the four-day February 2009 period. Heavy precipitation occurred over

northern Ivory Coast, southeastern Guinea and southern Mali, with light precipitation extending across the Sahel far into the southern Sahara. These rainfalls were preceded by a wave-breaking event over the North Atlantic that generated a trough with a strongly positive tilt in the horizontal over Morocco and Algeria on 16 February 2009 (marked in figure). Tight gradients in the geopotential at 300 hPa all across northern Africa indicate a subtropical jet streak. The mean sea-level pressure (MSLP) falls significantly to the southeast of the trough (i.e., in the right entrance region of the jet streak), leading to a northward shift of the weak wintertime heat low to eastern Burkina Faso on 16 February 2009 ("X" in figure), 5° to the north of its climatological position. The associated enhanced north–south MSLP gradient at its equatorward flank allows moist air from the Gulf of Guinea to penetrate farther than usual into the continent and feed the rainfall. The upper-trough drifts southwestward along the northwest African coast until 19 February while the surface low slowly weakens (not shown). The resulting rainfall is mainly related to rather short-lived cellular convection during the afternoon and evening of 16–18 February and a slightly more organized system in the early morning hours of 19 February. These systems occur at the southern end of an extended southwest–northeast-oriented cloud band [a so called 'tropical plume', see *Knippertz*, 2007], which drifts very slowly westward during 16–20 February in connection with the movement of the upper-trough (Figure 15c). A vertical cross section through this plume showing Cloudsat radar reflectivity (Figure 15d) indicates a sudden south–north decrease in cloud top height and three bands of precipitation Strong evaporation at low levels, however, inhibits significant accumulations (Figure 15a).

Consistent with results by Knippertz and Fink [2009], the general northward shift of the rain zone was reasonably well predicted with five day leads by the ECMWF. Despite this, the relative contributions of dynamical versus diabatic processes to the pressure fall are not well understood [*Knippertz and Fink*, 2008], and details of the associated moisture inflow from the Gulf of Guinea and the ensuing tropical convection challenge present-day forecast models. Note the synergistic use of the high resolution ECMWF YOTC analyses, station measurements and satellite data to develop a robust characterization of this multi-faceted and impactful event – a capability that YOTC objectives are focused on facilitating (see M10).

6.3 Atmospheric Rivers

Atmospheric rivers (ARs) play a key role in the tropical-extratropical water cycle. Occupying ~10% of the earth's circumference in the midlatitudes, they account for over 90% of the poleward moisture transport [*Zhu and Newell*, 1994; 1998]. They largely form in the extra-tropical ocean basins north of the tropical moisture reservoir. Some ARs are more directly linked to the deep tropics than others. Landfalling ARs often lead to enhanced precipitation in the mountains of the west coast of North America, and are responsible for some extreme precipitation/flood events in the region [*Ralph et al.*, 2006; *Neiman et al.*, 2008a]. Detection of ARs involves identifying narrow channels of enhanced moisture, typically identified in satellite observations of integrated water vapor (IWV) [*Ralph et al.*, 2004; *Neiman et al.*, 2008b]. For this overview of the ARs during YOTC, daily maps of IWV from the Atmospheric InfraRed Sounder (AIRS) were manually examined for AR-like structures (i.e., moisture plumes with 2 cm or greater IWV, narrower than 1000 km and longer than about 2000 km; [*Ralph et al.*, 2004]). Approximate locations of the ARs identified are shown in Figure 16 for the two half periods (i.e. years) of YOTC.[5] A total of 259 ARs are identified, with 122 and 137 during each half period. In the first year, the maximum number of

[5] AIRS data are not available during 10–25 January 2010 due to hardware failure. AR detection was not performed for that period.

ARs occurred in the northeastern Pacific, with a similar number observed there in the second year. The southeastern Pacific, on the other hand, saw an increase of 70% in the number of ARs in the second year. This is likely to be an influence of ENSO but the manner this may be so has not been established. Noteworthy is the scarcity of landfalling ARs in California during the YOTC period, as the average occurrence is about 15 per year [*Neiman et al.*, 2008b].

The impact of landfalling ARs is illustrated in Figure 17 with an example of an extreme precipitation event in California's Sierra Nevada mountains. There, a few AR events can result in as large as 40% of the total seasonal snow accumulation (Guan et al., in preparation)—an important water resource during summer. The figure shows the IWV plume and the 3-day cumulative precipitation associated with this event, which reached 9 cm on average[6]. A number of studies have showed the connection of the MJO to precipitation extremes in the U.S. West Coast and elsewhere [*Mo and Higgins*, 1998b; a; *Jones*, 2000; *Bond and Vecchi*, 2003]. Analysis of snow accumulation in the Sierra Nevada showed a preference of AR-related extreme events to occur when MJO activity is enhanced in the western Pacific [*Guan et al.*, 2010]. Three AR-related extreme precipitation events during YOTC (including the one discussed here) occurred during relatively weak MJOs (amplitude $\leq$ 1) in the Indian/Western Pacific Oceans. It remains to be explored and understood how conditions in the tropics, such as convection and circulation anomalies associated with MJO, affect the formation and impact of AR.

SIDEBAR: Shallow Convection Processes: A VOCALS and YOTC Overlap

Understanding shallow convection processes is critical to achieving better simulations and predictions associated with the expansive, low-level, high-albedo cloud regions of the tropics as well as of transitions between shallow and deep convection. A primary goal of the Variability of the American Monsoon Systems (VAMOS) Ocean-Cloud-Atmosphere-Land Study (VOCALS) Regional Experiment (REx) is to characterize the structural properties of the marine boundary layer (MBL) over the southeastern tropical Pacific (SEP). In particular, components of the VOCALS field campaign were designed to better characterize the dominant forms of mesoscale cellular convection (MCC), which in the SEP include closed cell and open cell structures, the latter with broken cloud and lower albedo. Pockets of open cells (POC) usually form within overcast closed MCC [*Bretherton et al.*, 2004; *Stevens et al.*, 2005; *Comstock et al.*, 2007; *Wood et al.*, 2008]. The transition from closed to open cells represents a shift from a system driven primarily by cloud-top longwave cooling to a more cumuliform structure in which lifting is in part forced at the surface by localized cold pools formed by the evaporation of drizzle [*Wang and Feingold*, 2009; *Feingold et al.*, 2010].

[6] Three high-impact (3-day cumulative precipitation > 9 cm in the Sierra Nevada) AR events in California were identified during the YOTC period. However, none of them strictly conformed to the Ralph et al. criteria in terms of length or overall structure, including the one discussed here which was 5% shorter than the criteria and thus isn't included in Figure 16. On the other hand, three ARs meeting the criteria were identified in California during YOTC, but all with low impact (3-day cumulative precipitation < 0.5 cm in the Sierra Nevada).

The intensive observational phase of VOCALS-REx took place during October and November 2008 and involved five aircraft, two ships and several ground sites [*Wood et al.*, 2010; *Wood et al.*, 2010a]. Satellite imagery of the 27/28 October 2008 POC event (Fig. 1a Sidebar) shows the formation of a POC aligned roughly NW-SE within overcast stratocumulus clouds early in the morning of 27 Oct. Ship radar observations (Fig 1b Sidebar) reveal locally intense drizzle cells surrounded by drizzle-free regions. The aircraft observations on the NE side sampled during the evening of 27 Oct and early morning of 28 Oct reveal marked transitions in drizzle structure, and in cloud and aerosol microphysical properties across the boundary [*Wood et al.*, 2010]. Ship radar observations in the overcast region to the SW of the POC revealed the presence of more diffusedrizzling cells (Fig 1c Sidebar), that have peak rain rates less than the echoes observed within the POC. Subsequently, the POC evolved by growing in width and advecting to the NW with the synoptic flow. The VOCALS-REx dataset, along with complementary elements of the YOTC project (see companion article M10), provide promising avenues for improving our basic understanding of these processes, including capturing their bulk effects in our global weather and climate models.

7 Summary

The discussion above highlights the diverse and impactful nature of the weather and climate associated with the WCRP-WWRP/THORPEX YOTC period of interest. Notable is the wide range of scale interactions involving tropical convection, particularly in terms of how the influence of ENSO cascades across a number of time scales and phenomena including significant impacts on most of the monsoon circulations discussed, the nature of the intraseasonal variability, the structure and intensity of easterly waves, as well as the spatial modulation of extreme events such as tropical cyclones and atmospheric rivers. Significant highlights apart from the cool to warm transition in ENSO, are the severe drought monsoon for India in 2009 and the near record setting N. American monsoon in 2008. There was a fantastic tropical wave event in 2008 that impacted monsoon onset(s) and extreme events in both the western and eastern hemisphere, and other examples of convectively-coupled wave-wave interactions. There were high impact rainfall events in Africa that derived from tropical sources (i.e. easterly waves) in both 2008 and 2009 and a number of cases that arose from the influence of the extratropics. The tropical cyclone activity during YOTC exhibited numerous highlights, including Ike – one of the largest storm ever recorded in aerial size in the Atlantic, Nargis - that led to disastrous consequences in Myanmar, three hurricanes making landfall onto Mexico from the Pacific in 2008, the 1.8 m of rainfall over the Philippines from slow moving Typhoon Parma, Rick – the second strongest hurricane on record in the Pacific, high latitude hurricane Grace tracking across the UK, and a highly unusual South Atlantic storm named Anita. Moreover, the impact of ETs on the midlatitude flow during the entire YOTC period exhibits substantial variability both in terms of the excitation of Rossby wavetrains and the predictive skill of this process. The objectives of YOTC are to highlight these types of features and phenomena and promote their interrogation via theory, observations and models so that improved understanding and predictions can be afforded.

With the backing of the World Climate Research Program and World Weather Research Program/THORPEX, the YOTC research program is developing a suite of state-of-the-art data sets to examine the aforementioned weather and climate highlights in more detail. These include high-resolution atmospheric analyses from ECMWF, NCEP and NASA and a number of satellite data products including a multi-sensor co-located dataset based on the Earth Observing System's A-

Train. Moreover, the YOTC period occurred in conjunction with the T-PARC and VOCALS field programs as well as a multitude of activities associated with the Asian Monsoon Year (AMY), all of which allow additional resources and focus to be brought to bear on interrelated tropical convection issues. By leveraging these activities and resources, the YOTC Implementation Plan sets a course to develop a number of programmatic research activities, model studies and intercomparisons. One particular focus is on using models in hindcast mode to explore their sensitivities and shortcomings in conjunction with the above observation resources to drive at improvements in our forecast capabilities from short-term to seasonal prediction. This program and its focus provide an initial framework to develop the techniques and know-how to approach the next generation of high-resolution models (e.g., global CSRMs, MMF, regional and adaptive grid systems) that at present tax our abilities to fully exploit all our resources – both in terms of technical (e.g. network and analysis bandwidth) and scientific (multi-scale interactions, multi-sensor constraints/evaluation) challenges. In this regard, YOTC provides an excellent and rich activity through which to entrain and train the next generation of weather, climate and Earth scientists. This new generation will be ideally situated to capitalize on the new capabilities that have and are being put into place, including the interdisciplinary education and landscape being established to tackle the pressing environmental and societally impactful challenges associated with tropical convection. For additional motivation, scientific underpinnings and hypotheses associated with YOTC, see M10.

ACKNOWLEDGEMENTS

This research has been supported by the National Science Foundation, Mesoscale Dynamic Meteorology Program, under Grant No. ATM-0639461 and the National Oceanic and Atmospheric Administration, Office of Global Programs, under Grant No. NA07OAR4310263. The European Centre for Medium-Range Weather Forecasts is acknowledged for providing the special ECMWF YOTC data set. We thank Paul Ciesielski and Andy Newman for assistance in the preparation of figures. The Cloudsat and TRMM data were visualized with the Giovanni online data system, developed and maintained by the NASA GES DISC. The Meteosat image was downloaded from the webpage of the Dundee Satellite Receiving Station. We are grateful to the ECMWF for providing access to the YOTC analysis and forecast products, and to the French IRD and the National Weather Services of Benin, Guinea, and Ghana for providing rainfall data for February 2009. BNG thanks Neena Mani Joseph and Suhas E for help in creating the Indian Monsoon figures. YLS was supported by NOAA's Climate Program Office under grant NA06OAR43100. DJG was supported by NOAA Climate Program Office Grant No. NA08OAR4310705.

REFERENCES

Ajayamohan, R. S., S. A. Rao, J.-J. Luo, and T. Yamagata (2009), Influence of Indian Ocean Dipole on boreal summer intraseasonal oscillations in a CGCM, Journal of Geophysical Research, 114, D06119, doi:10.1029/2008JD011096.

Ambaum, M. H. P., B. J. Hoskins, and D. B. Stephenson (2001), Arctic oscillation or North Atlantic oscillation?, Journal of Climate, 14(16), 3495-3507.

Anwender, D., P. A. Harr, and S. C. Jones (2008), Predictability associated with the downstream impacts of the extratropical transition of tropical cyclones: Case studies, Monthly Weather Review, 136(9), 3226-3247.

Black, E., J. Slingo, and K. R. Sperber (2003), An Observational Study of the Relationship between Excessively Strong Short Rains in Coastal East Africa and Indian Ocean SST., Monthly Weather Review, 131(1): 74.

Bond, N. A., and G. A. Vecchi (2003), The influence of the Madden-Julian oscillation on precipitation in Oregon and Washington, Weather and Forecasting, 18(4), 600-613.

Bretherton, C. S., T. Uttal, C. W. Fairall, S. E. Yuter, R. A. Weller, D. Baumgardner, K. Comstock, R. Wood, and G. B. Raga (2004), The EPIC 2001 stratocumulus study, Bulletin of the American Meteorological Society, 85(7), 967-+.

Castro, C. L., T. B. McKee, and R. A. Pielke (2001), The relationship of the North American monsoon to tropical and North Pacific sea surface temperatures as revealed by observational analyses. , J. Climate, 14, 4449-4473.

Cavazos, T., and S. Hastenrath (1990), CONVECTION AND RAINFALL OVER MEXICO AND THEIR MODULATION BY THE SOUTHERN OSCILLATION, International Journal of Climatology, 10(4), 377-386.

Comstock, K. K., S. E. Yuter, R. Wood, and C. S. Bretherton (2007), The three-dimensional structure and kinematics of drizzling stratocumulus, Monthly Weather Review, 135(11), 3767-3784.

Drosdowsky, W. (1996), Variability of the Australian summer monsoon at Darwin: 1957-1992, Journal of Climate, 9(1), 85-96.

Englehart, P. J., and A. V. Douglas (2001), The role of eastern North Pacific tropical storms in the rainfall climatology of western Mexico, International Journal of Climatology, 21(11), 1357-1370.

Feingold, G., I. Koren, H. Wang, H. Xue, and W. A. Brewer (2010), Precipitation-generated oscillations in open cellular cloud fields, Nature, 466, 849–852, doi:10.1038.

Fink, A. H., J. M. Schrage, and S. Kothaus (2010), On the Potential Causes of the Nonstationary Correlations between West African Precipitation and Atlantic Hurricane Activity, Journal of climate, In Press.

Flatau, M. K., P. J. Flatau, and D. Rudnick (2001), The Dynamics of Double Monsoon Onsets, Journal of Climate, 14, 4130–4146.

Giannini, A., M. A. Cane, and Y. Kushnir (2001), Interdecadal changes in the ENSO teleconnection to the Caribbean region and the North Atlantic oscillation, Journal of Climate, 14(13), 2867-2879.

Gochis, D. J., L. Brito-Castillo, and W. J. Shuttleworth (2007), Correlations between sea-surface temperatures and warm season streamflow in northwest Mexico, International Journal of Climatology, 27(7), 883-901.

Gochis, D. J., S. W. Nesbitt, W. Yu, and S. F. Williams (2009), Comparison of gauge-corrected

versus non-gauge corrected satellite-based quantitative precipitation estimates during the 2004 NAME enhanced observing period, Atmosfera, 22(1), 69-98.
Guan, B., N. P. Molotch, D. E. Waliser, E. J. Fetzer, P. J. Neiman, and Geophys. Res. Lett. (2010), Extreme snowfall events linked to atmospheric rivers and surface air temperature via satellite measurements, Geophys. Res. Lett., doi:10.1029/2010GL044696.
Harr, P. A., D. Anwender, and S. C. Jones (2008), Predictability associated with the downstream impacts of the extratropical transition of tropical cyclones: Methodology and a case study of Typhoon Nabi (2005), Monthly Weather Review, 136(9), 3205-3225.
Harr, P. A., and J. M. Dea (2009), Downstream Development Associated with the Extratropical Transition of Tropical Cyclones over the Western North Pacific, Monthly Weather Review, 137(4), 1295-1319.
Hastenrath, S., and L. Greischar (2001), The North Atlantic oscillation in the NCEP-NCAR reanalysis, Journal of Climate, 14(11), 2404-2413.
Hendon, H. H., C. D. Zhang, and J. D. Glick (1999), Interannual variation of the Madden-Julian oscillation during austral summer, Journal of Climate, 12(8), 2538-2550.
Hendon, H. H., M. C. Wheeler, and C. D. Zhang (2007), Seasonal dependence of the MJO-ENSO relationship, Journal of Climate, 20(3), 531-543.
Higgins, R. W., K. C. Mo, and Y. Yao (1998), Interannual variability of the US summer precipitation regime with emphasis on the southwestern monsoon, Journal of Climate, 11(10), 2582-2606.
Higgins, R. W., W. Shi, and C. Hain (2004), Relationships between Gulf of California moisture surges and precipitation in the southwestern United States, Journal of Climate, 17(15), 2983-2997.
Horel, J. D., and J. M. Wallace (1982), Planetary-Scale Atmospheric Phenomena Associated with the Southern Oscillation - Reply, Monthly Weather Review, 110(10), 1497-1497.
Hsu, P. C., C. H. Tsou, H. H. Hsu, and J. H. Chen (2009), Eddy Energy along the Tropical Storm Track in Association with ENSO, Journal of the Meteorological Society of Japan, 87(4), 687-704.
Huffman, G. J., R. F. Adler, D. T. Bolvin, G. Gu, E. J. Nelkin, K. P. Bowman, Y. Hong, E. F. Stocker, and D. B. Wolff (2007), The TRMM Multisatellite Precipitation Analysis (TMPA): Quasi-Global, Multiyear, Combined-Sensor Precipitation Estimates at Fine Scales, Journal of Hydrometeorology, 8(1), 38-55.
Janiga, M. A. (2010), Easterly wave structural evolution over West Africa and the East Atlantic, paper presented at 29th Conference on Hurricanes and Tropical Meteorology, Tuscon, AZ, May, 2010.
Jones, C. (2000), Occurrence of extreme precipitation events in California and relationships with the Madden-Julian oscillation, Journal of Climate, 13(20), 3576-3587.
Jones, S. C., P. A. Harr, J. Abraham, L. F. Bosart, P. J. Bowyer, J. L. Evans, D. E. Hanley, B. N. Hanstrum, R. E. Hart, F. Lalaurette, M. R. Sinclair, R. K. Smith, and C. Thorncroft (2003), The extratropical transition of tropical cyclones: Forecast challenges, current understanding, and future directions, Weather and Forecasting, 18(6), 1052-1092.
Joseph, S., A. K. Sahai, and B. N. Goswami (2009), Boreal summer intraseasonal oscillations and seasonal Indian monsoon prediction in DEMETER coupled models, Climate Dynamics, DOI 10.1007/s00382-009-0635-3.
Kessler, W. S. (2001), EOF representations of the Madden-Julian oscillation and its connection with ENSO, Journal of Climate, 14(13), 3055-3061.
Kiladis, G. N., C. D. Thorncroft, and N. M. J. Hall (2006), Three-dimensional structure and

dynamics of African easterly waves. Part I: Observations, Journal of the Atmospheric Sciences, 63(9), 2212-2230.
Kiladis, G. N., M. C. Wheeler, P. T. Haertel, K. H. Straub, and P. E. Roundy (2009), CONVECTIVELY COUPLED EQUATORIAL WAVES, Reviews of Geophysics, 47.
Knippertz, P., and J. E. Martin (2005), Tropical plumes and extreme precipitation in subtropical and tropical West Africa, Quarterly Journal of the Royal Meteorological Society, 131(610), 2337-2365.
Knippertz, P. (2007), Tropical-extratropical interactions related to upper-level troughs at low latitudes, Dynamics of Atmospheres and Oceans, 43(1-2), 36-62.
Knippertz, P., and A. H. Fink (2008), Dry-season precipitation in tropical West Africa and its relation to forcing from the extratropics, Monthly Weather Review, 136(9), 3579-3596.
Knippertz, P., and A. H. Fink (2009), Prediction of Dry-Season Precipitation in Tropical West Africa and Its Relation to Forcing from the Extratropics, Weather and Forecasting, 24(4), 1064-1084.
Kumar, A., and M. P. Hoerling (1998), Annual cycle of Pacific North American seasonal predictability associated with different phases of ENSO, Journal of Climate, 11(12), 3295-3308.
Lau, W. K. M. (2005), ENSO Connections, in Intraseasonal Variability of the Atmosphere-Ocean Climate System, edited by W. K. M. Lau and D. E. Waliser, Springer, Heidelberg, Germany.
Lau, W. K. M., and D. E. Waliser (Eds.) (2005), Intraseasonal Variability of the Atmosphere-Ocean Climate System, 474 pp., Springer, Heidelberg, Germany.
Liebmann, B., I. Blade, N. A. Bond, D. Gochis, D. Allured, and G. T. Bates (2008), Characteristics of north American summertime rainfall with emphasis on the monsoon, Journal of Climate, 21(6), 1277-1294.
Madden, R. A., and P. R. Julian (1971), Detection of a 40-50 Day Oscillation in Zonal Wind in Tropical Pacific, Journal of the Atmospheric Sciences, 28(5), 702-&.
Marengo, J., B. Liebmann, A. M. Grimm, V. Misra, P. L. S. Dias, I. F. A. Cavalcanti, L. V. Carvalho, E. B. Berbery, T. Ambrizzi, C. Vera, J. Nogues-Paegle, E. Zipser, and A. Seth (2010), New developments on the functioning, characteristics and variability of the South American Monsoon System,, Int. J. Climatology, In press.
Marengo. J., B. Liebmann, A. M. Grimm, V. Misra, P. L. Silva Dias, I. F. A. Cavalcanti, L. V. Carvalho, E. B. Berbery, T. Ambrizzi, C. Vera, J. Nogues-Paegle, E. Zipser, and A. Seth (2010), New developments on the functioning, characteristics and variability of the South American Monsoon System,, Int. J. Climatology, In press.
Meier, F., and P. Knippertz (2009), Dynamics and Predictability of a Heavy Dry-Season Precipitation Event over West Africa-Sensitivity Experiments with a Global Model, Monthly Weather Review, 137(1), 189-206.
Mo, K. C., and R. W. Higgins (1998a), Tropical convection and precipitation regimes in the western United States, Journal of Climate, 11(9), 2404-2423.
Mo, K. C., and R. W. Higgins (1998b), Tropical influences on California precipitation, Journal of Climate, 11(3), 412-430.
Moncrieff, M. W., M. Shapiro, J. Slingo, and F. Molteni (2007), Collaborative research at the intersection of weather and climate, WMO Bulletin, 56, 204-211.
Neiman, P. J., F. M. Ralph, G. A. Wick, Y. H. Kuo, T. K. Wee, Z. Z. Ma, G. H. Taylor, and M. D. Dettinger (2008a), Diagnosis of an Intense Atmospheric River Impacting the Pacific Northwest: Storm Summary and Offshore Vertical Structure Observed with COSMIC

Satellite Retrievals, Monthly Weather Review, 136(11), 4398-4420.
Neiman, P. J., F. M. Ralph, G. A. Wick, J. D. Lundquist, and M. D. Dettinger (2008b), Meteorological characteristics and overland precipitation impacts of atmospheric rivers affecting the West Coast of North America based on eight years of SSM/I satellite observations, Journal of Hydrometeorology, 9(1), 22-47.
Newman, M., and P. D. Sardeshmukh (1998), The impact of the annual cycle on the North Pacific North American response to remote low-frequency forcing, Journal of the Atmospheric Sciences, 55(8), 1336-1353.
Nicholls, N., J. L. McBride, and R. J. Ormerod (1982), ON PREDICTING THE ONSET OF THE AUSTRALIAN WET SEASON AT DARWIN, Monthly Weather Review, 110(1), 14-17.
Ostermeier, G. M., and J. M. Wallace (2003), Trends in the North Atlantic Oscillation-Northern Hemisphere annular mode during the twentieth century, Journal of Climate, 16(2), 336-341.
Pope, M., C. Jakob, and M. J. Reeder (2009), Regimes of the North Australian Wet Season, Journal of Climate, 22(24), 6699-6715.
Ralph, F. M., P. J. Neiman, and G. A. Wick (2004), Satellite and CALJET aircraft observations of atmospheric rivers over the eastern north pacific ocean during the winter of 1997/98, Monthly Weather Review, 132(7), 1721-1745.
Ralph, F. M., P. J. Neiman, G. A. Wick, S. I. Gutman, M. D. Dettinger, D. R. Cayan, and A. B. White (2006), Flooding on California's Russian River: Role of atmospheric rivers, Geophysical Research Letters, 33(13).
Rao, S. A., S. Masson, J.-J. Luo, S. K. Behera, and T. Yamagata (2007), Termination of Indian Ocean Dipole events in a coupled general circulation model., Journal of Climate, 20, 3018–3035, doi:10.1175/JCLI4164.1.
Renwick, J. A., and J. M. Wallace (1996), Relationships between North Pacific wintertime blocking, El Nino, and the PNA pattern, Monthly Weather Review, 124(9), 2071-2076.
Saji, N. H., B. N. Goswami, P. N. Vinayachandran, and T. Yamagata (1999), A dipole mode in the tropical Indian Ocean, Nature, 401(6751), 360-363.
Serra, Y. (2009), Easterly wave activity and its modulation by the larger scales during the YOTC time period of focus: May 2008-Oct 2009, YOTC Session, American Geophysical Union Annual Meeting, San Francisco, CA, Dec., 2009.
Serra, Y. L., G. N. Kiladis, and M. F. Cronin (2008), Horizontal and vertical structure of easterly waves in the Pacific ITCZ, Journal of the Atmospheric Sciences, 65(4), 1266-1284.
Stevens, B., G. Vali, K. Comstock, R. Wood, M. C. van Zanten, P. H. Austin, C. S. Bretherton, and D. H. Lenschow (2005), Pockets of open cells and drizzle in marine stratocumulus, Bulletin of the American Meteorological Society, 86(1), 51-+.
Thorncroft, C., and K. Hodges (2001), African Easterly Wave Variability and Its Relationship to Atantic Tropical Cyclone Activity, J. Climate, 14, 116-1179.
Vera, C., W. Higgins, J. Amador, T. Ambrizzi, R. Garreaud, D. Gochis, D. Gutzler, D. Lettenmaier, J. Marengo, C. R. Mechoso, J. Nogues-Paegle, P. L. S. Dias, and C. Zhang (2006), Toward a unified view of the American Monsoon Systems, Journal of Climate, 19(20), 4977-5000.
Waliser, D., Z. Zhang, K. M. Lau, and J. H. Kim (2001), Interannual Sea Surface Temperature Variability and the Predictability of Tropical Intraseasonal Variability., Journal of the Atmospheric Sciences, 58, 2595-2614.
Waliser, D. E., and M. Moncrieff (2008), The Year of Tropical Convection (YOTC) Science

Plan: A joint WCRP - WWRP/THORPEX International Initiative. , WMO/TD No. 1452, WCRP - 130, WWRP/THORPEX - No 9. WMO, Geneva, Switzerland.
Wallace, J. M. (2000), North Atlantic Oscillation/annular mode: Two paradigms - one phenomenon, Quarterly Journal of the Royal Meteorological Society, 126(564), 791-805.
Wang, C. Z., S. K. Lee, and D. B. Enfield (2008), Atlantic Warm Pool acting as a link between Atlantic Multidecadal Oscillation and Atlantic tropical cyclone activity, Geochemistry Geophysics Geosystems, 9.
Wang, H. L., and G. Feingold (2009), Modeling Mesoscale Cellular Structures and Drizzle in Marine Stratocumulus. Part I: Impact of Drizzle on the Formation and Evolution of Open Cells, Journal of the Atmospheric Sciences, 66(11), 3237-3256.
Ward, M. N. (1998), Diagnosis and short-lead time prediction of summer rainfall in tropical North Africa at interannual and multidecadal timescales, Journal of Climate, 11(12), 3167-3191.
Wheeler, M., and G. N. Kiladis (1999), Convectively coupled equatorial waves: Analysis of clouds and temperature in the wavenumber-frequency domain, Journal of the Atmospheric Sciences, 56(3), 374-399.
Wheeler, M., and K. M. Weickmann (2001), Real-time monitoring and prediction of modes of coherent synoptic to intraseasonal tropical variability, Mon. Wea. Rev., 129, 2677-2694.
Wheeler, M. C., and H. H. Hendon (2004), An all-season real-time multivariate MJO index: Development of an index for monitoring and prediction, Monthly Weather Review, 132(8), 1917-1932.
Wood, R., K. K. Comstock, C. S. Bretherton, C. Cornish, J. Tomlinson, D. R. Collins, and C. Fairall (2008), Open cellular structure in marine stratocumulus sheets, Journal of Geophysical Research-Atmospheres, 113(D12).
Wood, R., C. S. Bretherton, D. Leon, A. D. Clarke, P. Zuidema, G. Allen, and H. Coe (2010), An aircraft case study of the spatial transition from closed to open mesoscale cellular convection, Atmos. Chem. Phys., Disc., 10, 17911-17980.
Wood, R., C. S. Bretherton, C. R. Mechoso, R. A. Weller, B. Huebert, F. Straneo, B. A. Albrecht, H. Coe, G. Allen, G. Vaughan, P. Daum, C. Fairall, D. Chand, L. G. Klenner, R. Garreaud, C. G. Quispe, D. S. Covert, T. S. Bates, R. Krejci, L. M. Russell, S. d. Szoeke, A. Brewer, S. E. Yuter, S. R. Springston, A. Chaigneau, T. Toniazzo, P. Minnis, R. Palikonda, S. J. Abel, W. O. J. Brown, S. Williams, J. Fochesatto, and J. Brioude (2010a), The VAMOS Ocean-Cloud-Atmosphere-Land Study Regional Experiment (VOCALS-REx): Goals, platforms, and field operations. , Atmos. Chem. Phys. Discuss., 10, 20769-20822.
Zhang, C. D. (2005), Madden-Julian Oscillation, Reviews of Geophysics, 43(2).
Zhu, Y., and R. E. Newell (1994), ATMOSPHERIC RIVERS AND BOMBS, Geophysical Research Letters, 21(18), 1999-2002.
Zhu, Y., and R. E. Newell (1998), A proposed algorithm for moisture fluxes from atmospheric rivers, Monthly Weather Review, 126(3), 725-735.

FIGURES

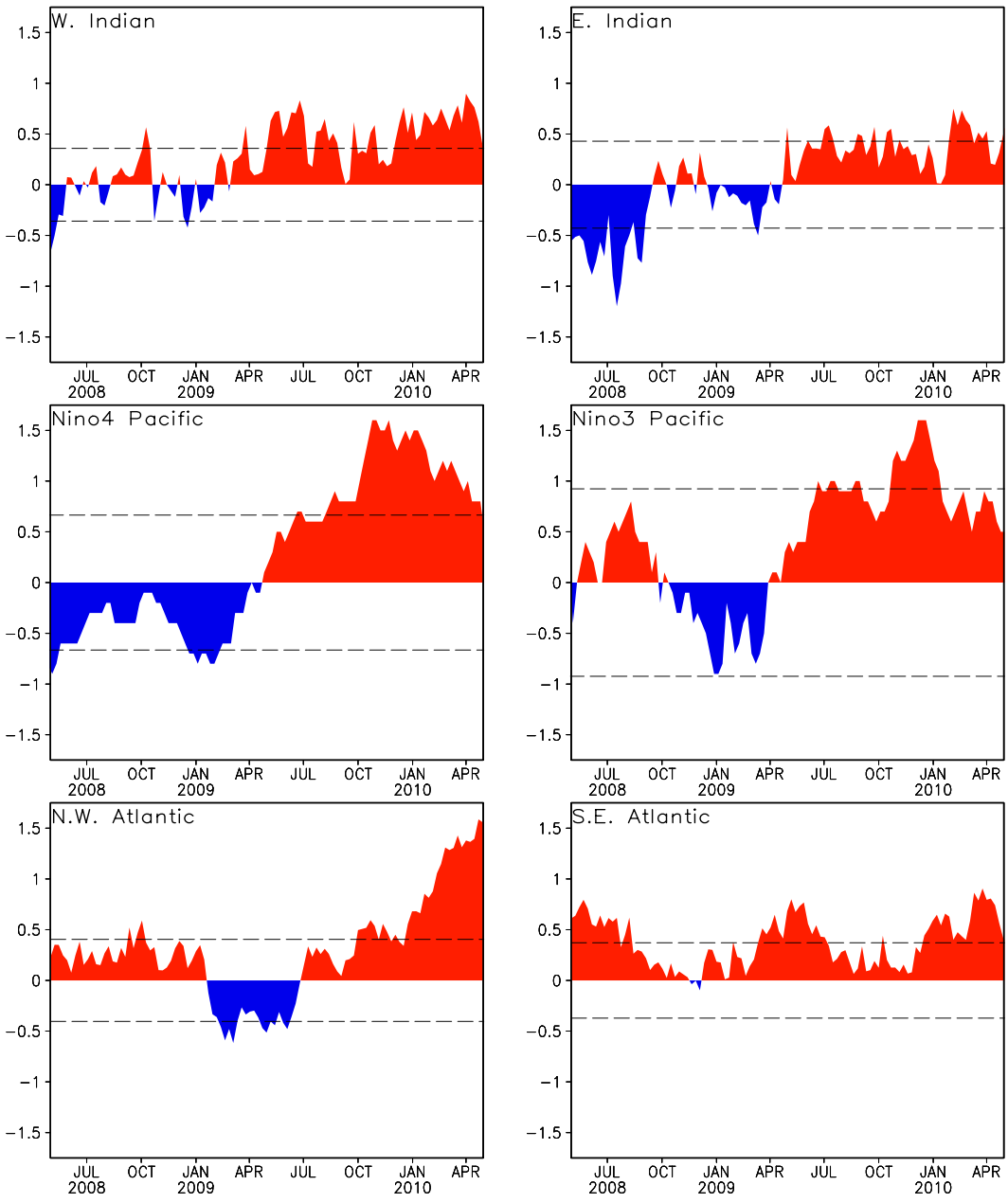

Figure 1. Tropical ocean SST anomalies in terms of weekly values during the YOTC period. (upper left) West Indian Ocean (50°E - 70°E, 10°S - 10°N), (upper right) East Indian Ocean (90°E - 110°E, 10°S - 0°), (middle left) Nino-4 160°E – (150°W, 5°S - 5°N), (middle right) Nino-3 (150°W - 90°W, 5°S - 5°N), (lower left) North Atlantic (55°W - 15°W, 5°N - 25°N), (lower right) South Atlantic (30°W - 10°E, 20°S - 0°).

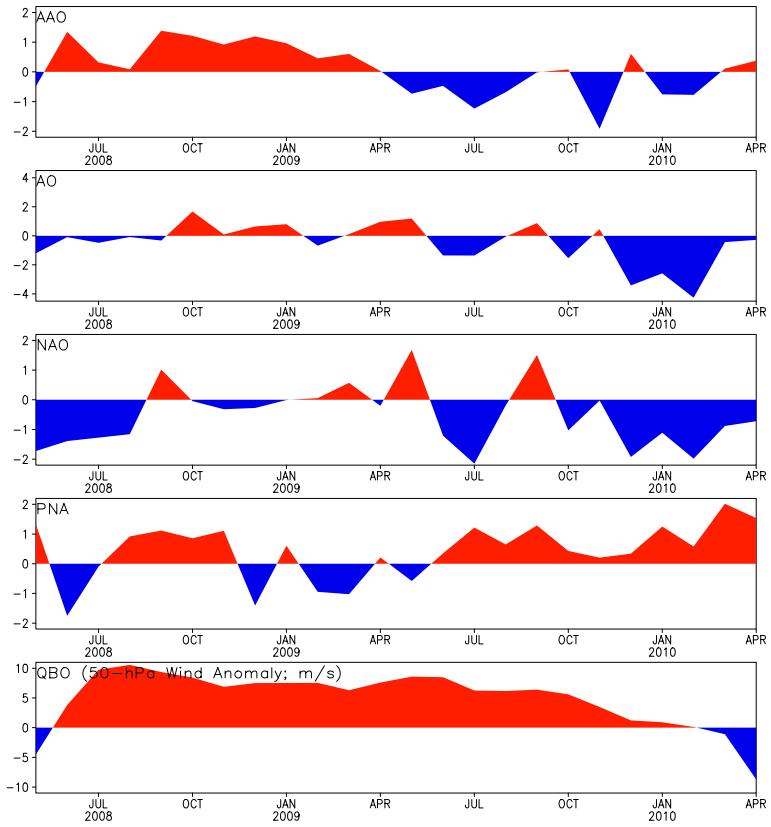

Figure 2. Time series of (from top to bottom) the AAO, AO, NAO, PNA and QBO for the YOTC period. Indices are defined and the data obtained from the following two CPC/NCEP/NOAA web sites (www.cpc.noaa.gov/data/indices/, www.cpc.ncep.noaa.gov/products /precip/CWlink/daily_ao_index/teleconnections.shtml).

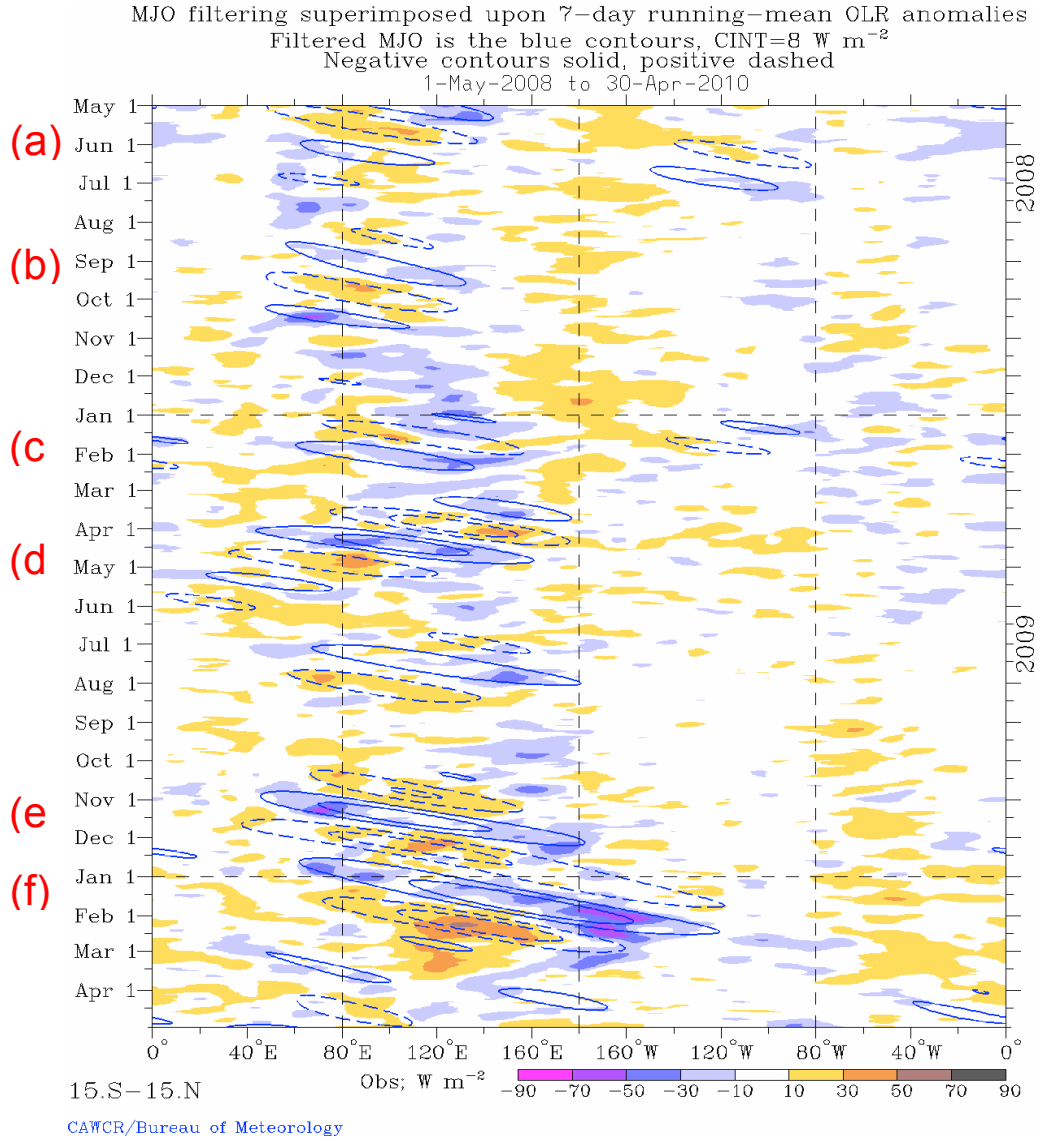

Figure 3. Time-longitude diagram of 15°S to15°N averaged OLR anomalies during the YOTC period, with MJO-filtered OLR anomalies superimposed. Shading is for "total" OLR anomalies which have been temporally (7-day running mean) and spatially (R21 spectral truncation) smoothed. Contours show OLR that has been wavenumber-frequency filtered for eastward-propagating waves 1-5 and periods 30-96 days as is used to signify convective variability associated with the MJO. Contour interval is 8 Wm^{-2} with dashed contours used for positive MJO-associated OLR anomalies. Labels (a)–(f) refer to the identified cases of MJO activity.

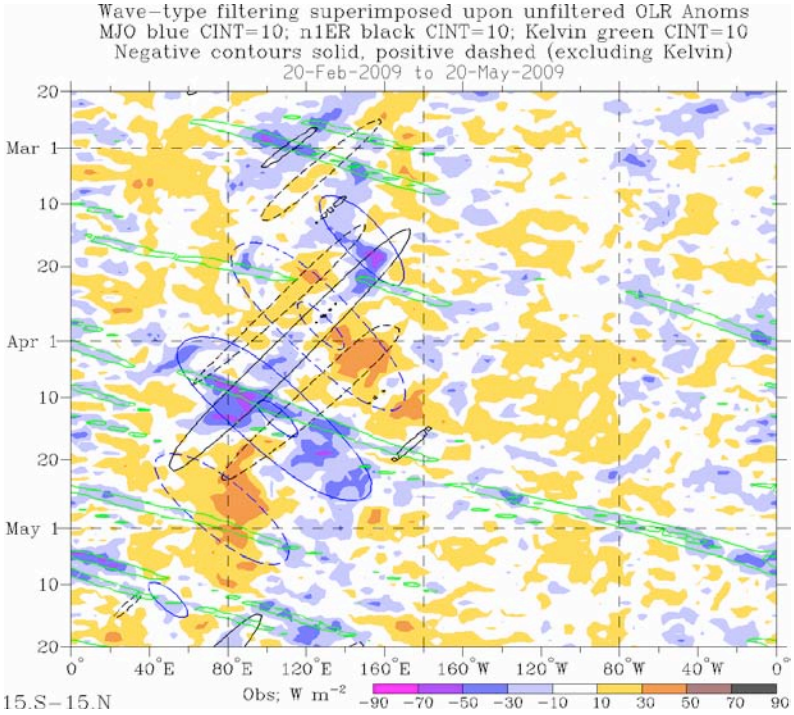

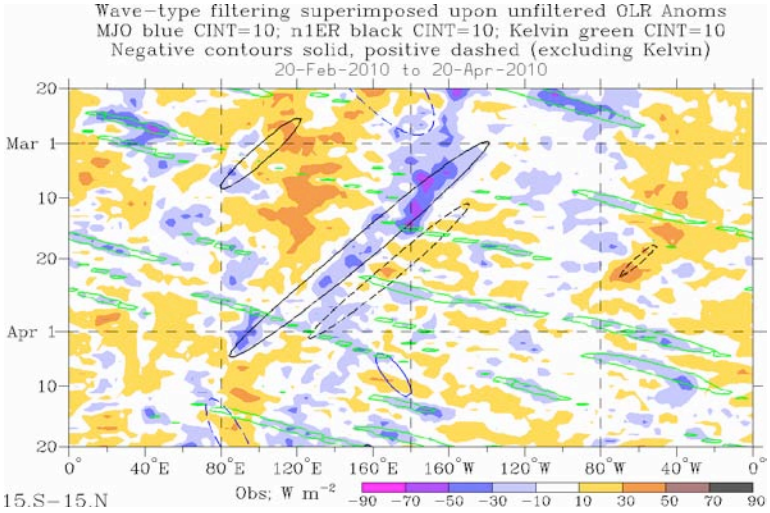

Figure 4. (top) 15°S to15°N-averaged OLR anomalies for the period 20 Feb-20 May 2009, during which multiple interacting waves (MJO, equatorial Rossby, and Kelvin) existed (CCEW case #1). Shading is for the unfiltered OLR anomalies, blue contours for the MJO-filtered OLR anomalies, black contours for the n=1 equatorial Rossby (ER) wave filtering, and green contours for the Kelvin wave filtering. Contour interval is 10 Wm^{-2}. Postive contours for the MJO and ER wave anomalies dashed, whereas for the Kelvin wave the positive contours are ommitted. (bottom) Same, except for the period 20 Feb-20 Apr 2010 (CCEW case #2).

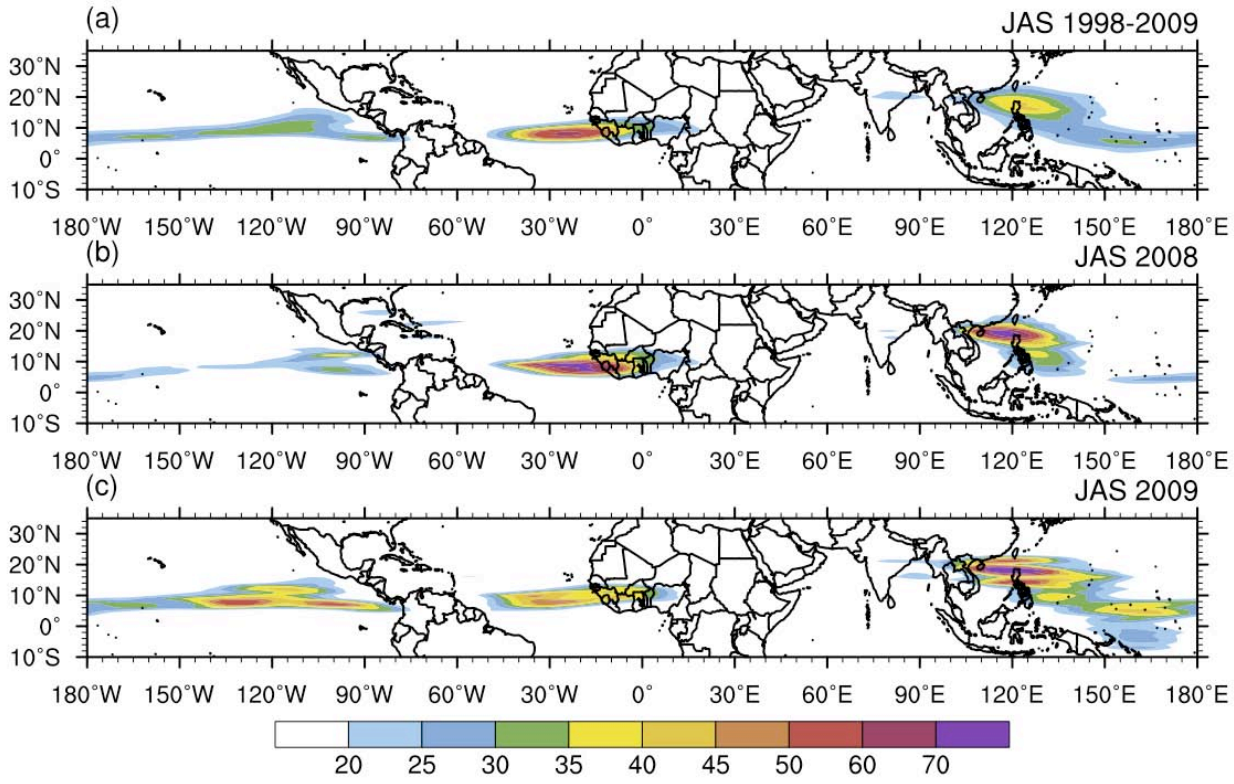

Figure 5. Variance of TRMM3B42 TD filtered rainrate for July-September averaged over (a) 1998-2009 (b) 2008, and (c) 2009.

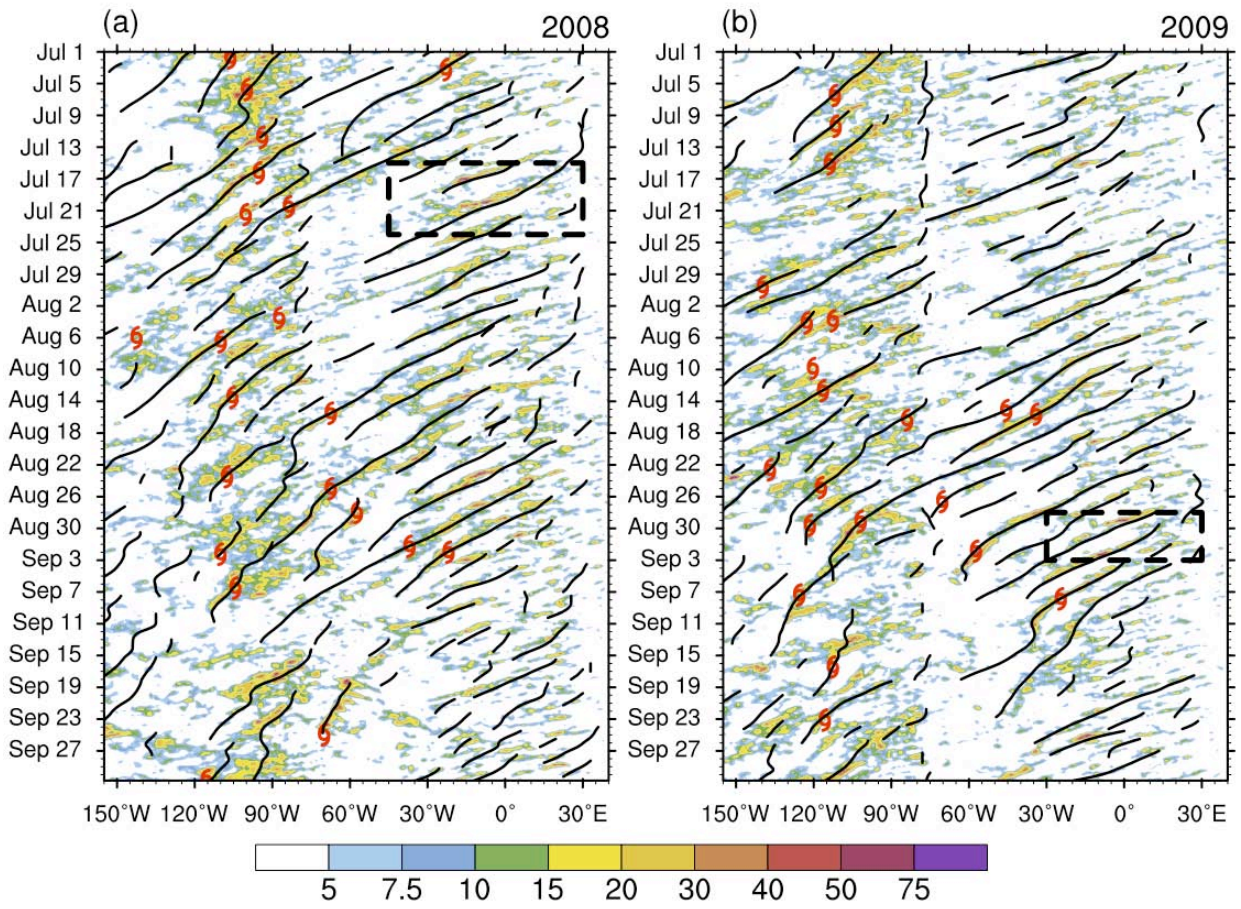

Figure 6. Hovmoller diagram of TRMM3B42 Rainrate (mm day-1, shaded) averaged between 5°-20°N and objective tracks of vorticity centers exceeding 1x10-5s^{-1} observed between 0°-30°N for (a) 2008 and (b) 2009. The time and longitude of named storm genesis is indicated by the red markers. Dashed boxes highlight periods of high impact weather referred to in the text.

a)

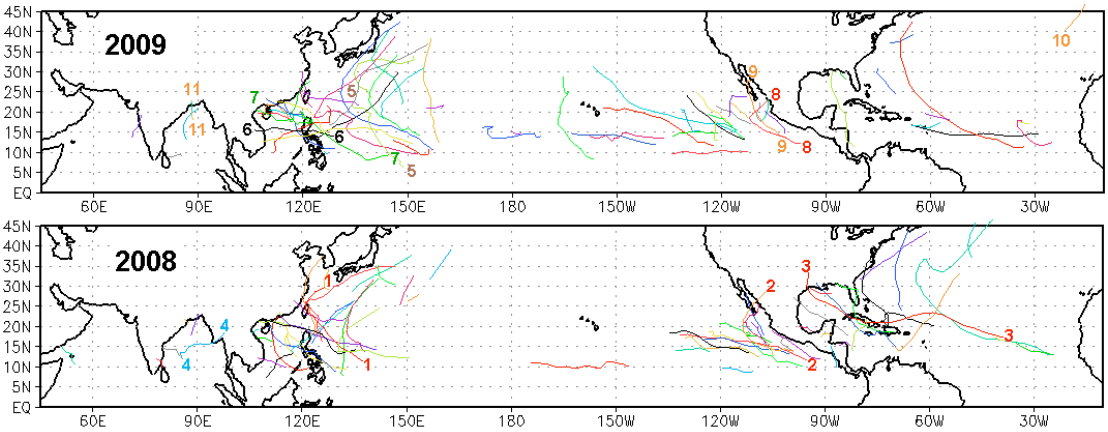

b)

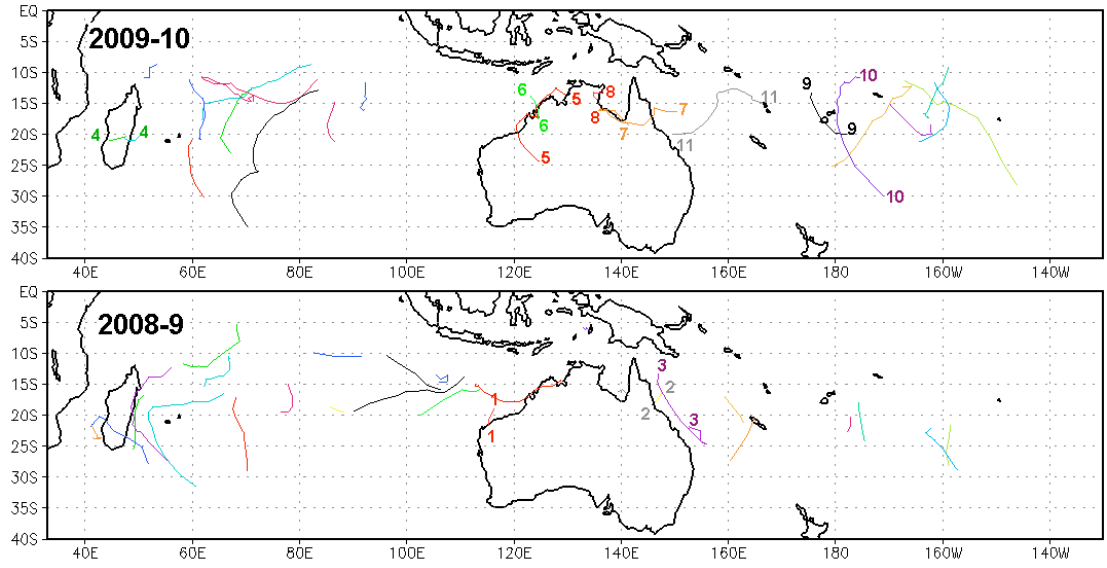

Figure 7. (a) Northern hemisphere tropical cyclone tracks. Top: 2009. Bottom: 2008. (b) Southern hemisphere tropical cyclone tracks. Top: 2009-10. Bottom: 2008-9.

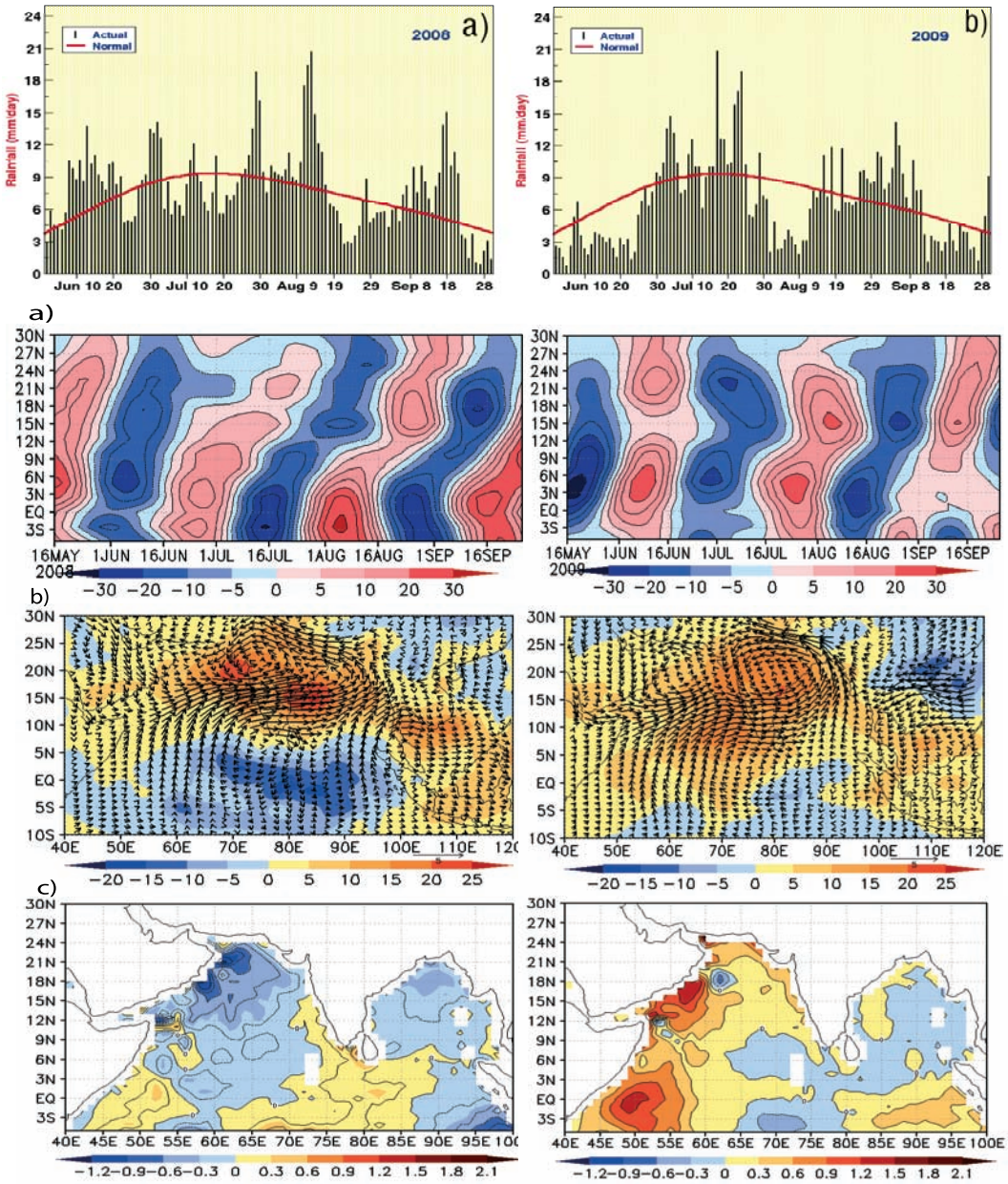

Figure 8. For all panels, left (right) side is 2008 (2009). (upper) All India monsoon rainfall daily variability during a) 2008 b) 2009 with long term mean (red curve). (upper middle) Northward propagation of 30-90 day filtered anomalies of OLR averaged over the longitude band 60E-90E. (lower middle)) Regressed structure of 10-90 day filtered OLR anomalies (shaded) and U850 anomalies against 10-90 day filtered OLR index averaged over central India (5-27.5N, 72.5-85E). (lower). June to September mean of TMI SST anomalies over the northern Indian Ocean region).

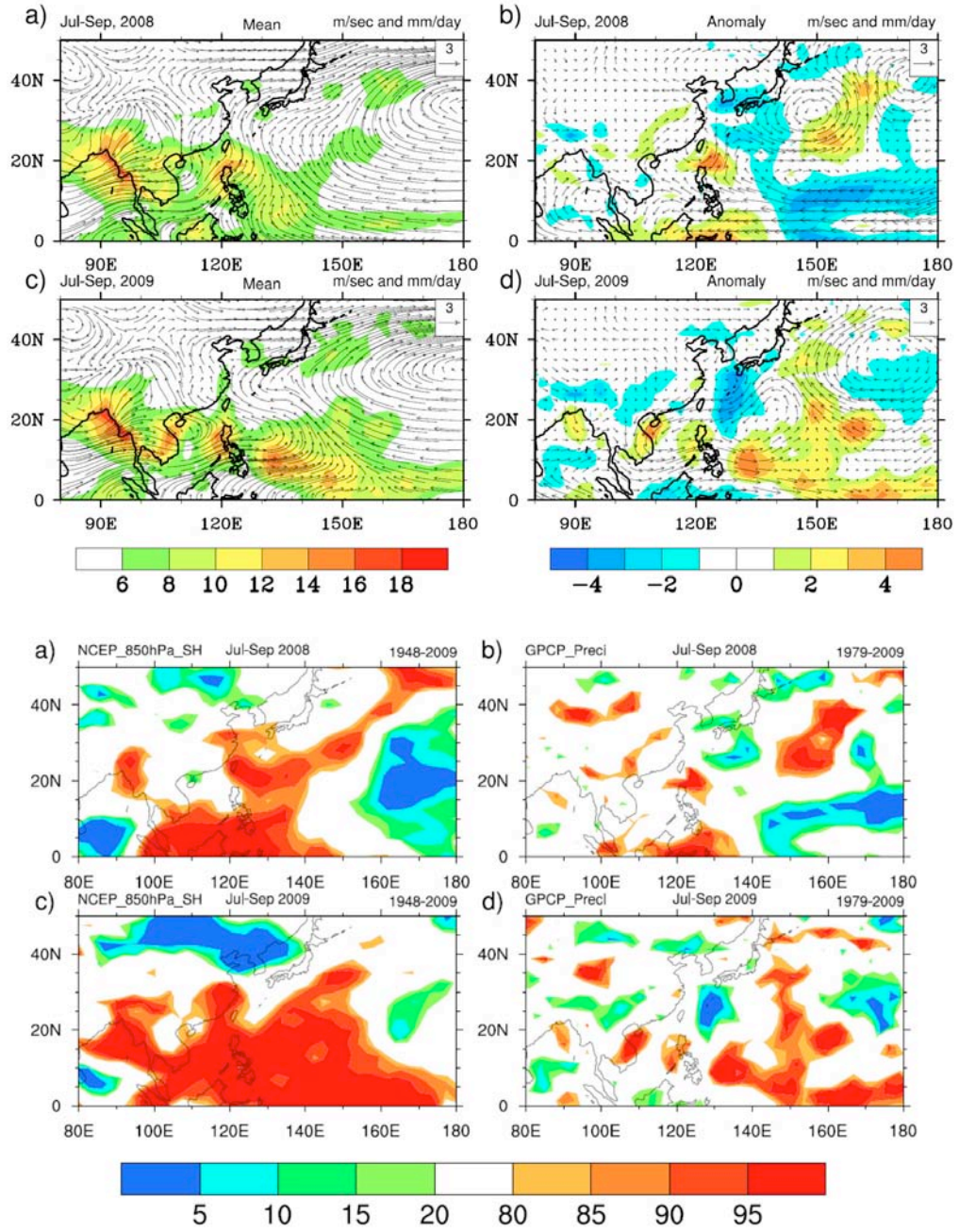

Figure 9. (top) Rainfall and 850-hPa Wind in July-September (a) 2008 and (c) 2009. (b, d) Same as in (c, d) except for anomaly. (bottom) Distribution of percentile for (a, c) 850 hPa specific humidity and (b, d) rainfall anomalies in July-September (a, b) 2008 and (c, d) 2009. Base periods for calculating percentile are 1949-2009 and 1979-2009 for specific humidity and rainfall, respectively.

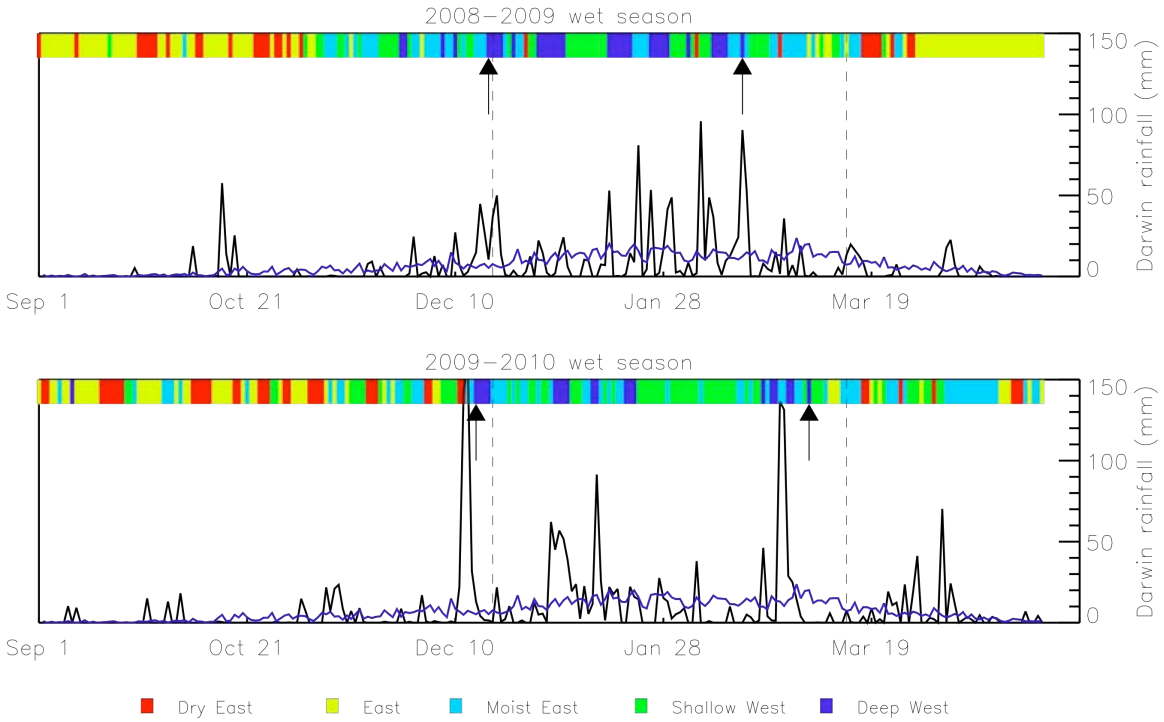

Figure 10 Time series of daily rainfall (black line) and daily wet-season regime (colour bar) for the NA wet seasons of 2008/09 (top) and 2009/10 (bottom). Also shown are the climatological rainfall distribution (blue line), the climatological monsoon onset and retreat days (vertical dashed lines) and the respective season's monsoon onset and retreat days (arrows) as defined in Pope et al. (2009).

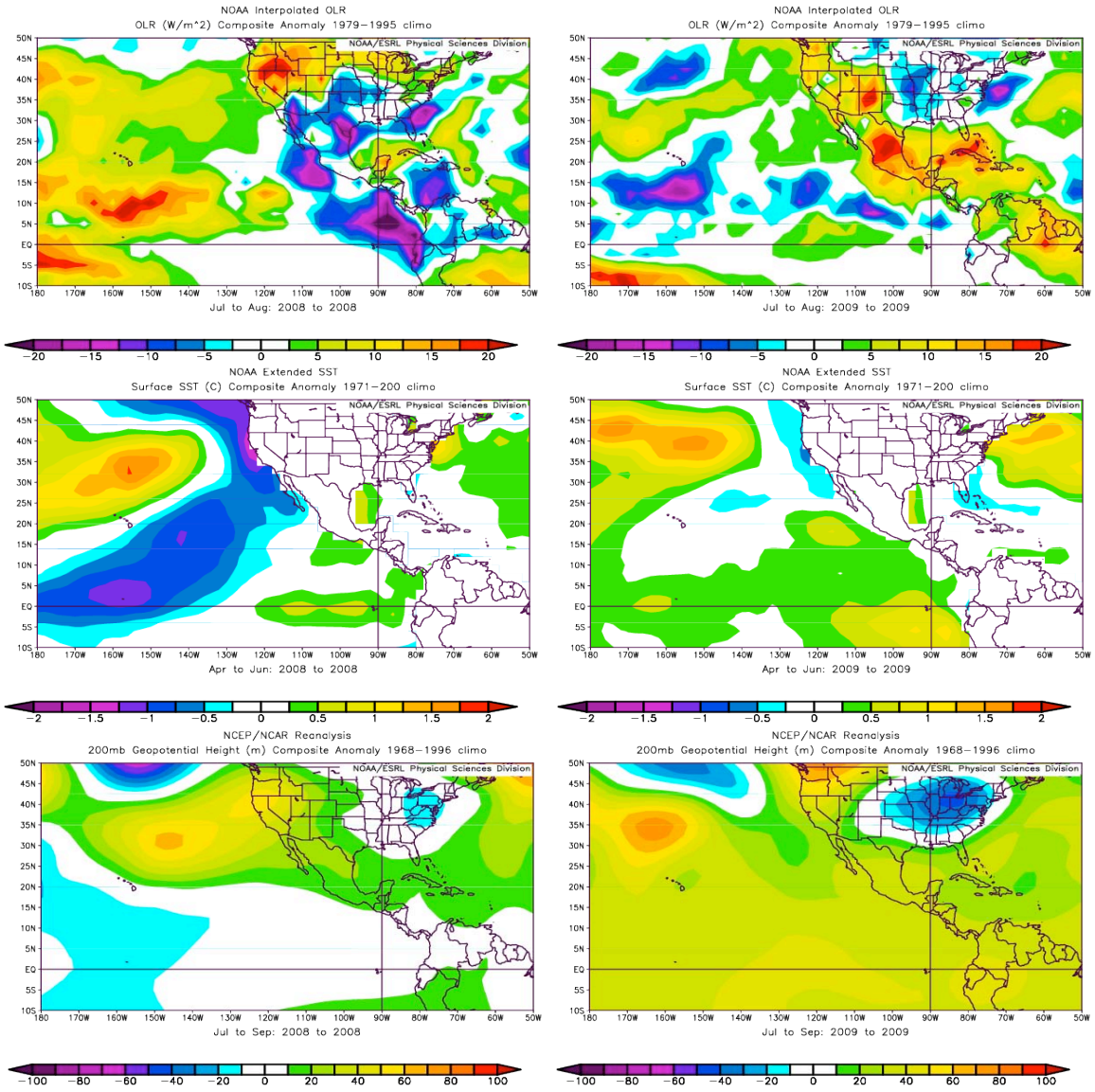

Figure 11. Jul-Aug NOAA interpolated OLR anomalies (a and b), antecedent season (Apr-May-June) NOAA Extended-OI sea surface temperature anomalies (c and d), and, Jul-Aug-Sep NCEP/NCAR reanalysis 200 hPa geopotential height anomalies (e and f) for 2008 and 2009, respectively.

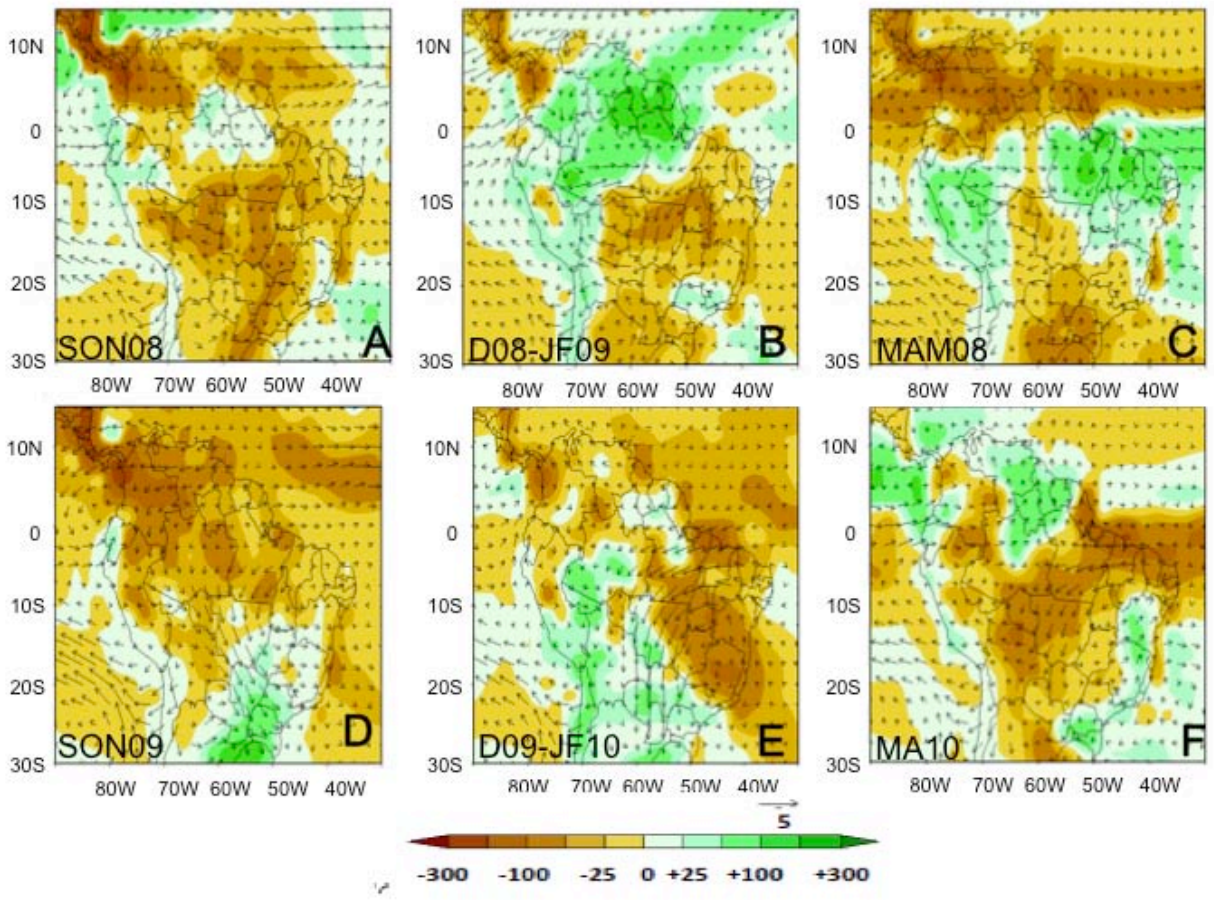

Figure 12. Rainfall and 850 hPa winds for the South American Monsoon system. Arrow indicating wind scale (m/s) and color scale (mm) are shown in the lower side of each panel. A)September-November 2008, B) December 2008-February 2009, C) March-May 2009, E) September-November 2009, F) December 2009-February 2010. Sources: CPTEC/INPE. São Paulo, Brazil, and CPC-NCEP/NOAA, Maryland, US

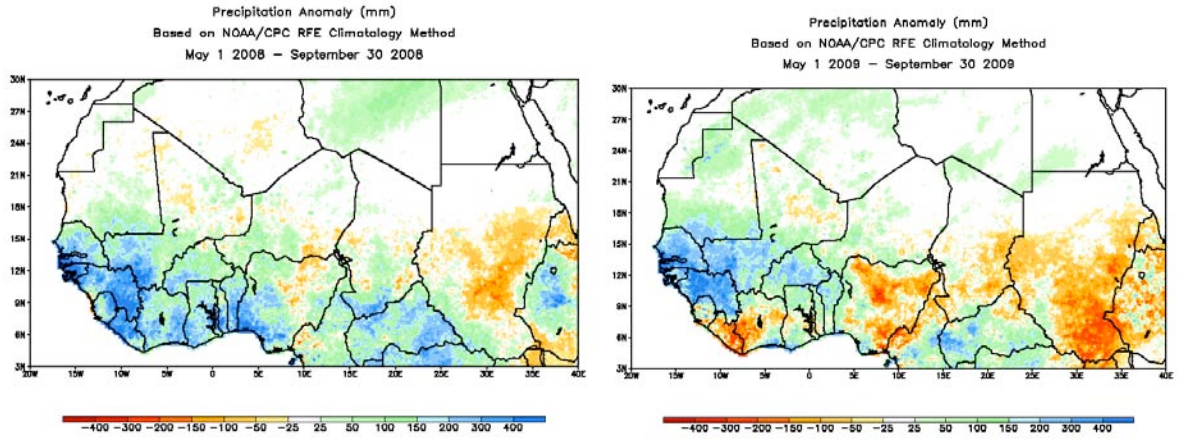

Figure 13. Seasonal precipitation anomalies for 2008 and 2009 based on May-September rainfall totals and with reference to a climatology based on the years 1995-2001. Precipitation is estimated using the NOAA/CPC RFE Climatology method (see http://www.cpc.noaa.gov/products/fews/AFR_CLIM/afr_clim_season.shtml for more details).

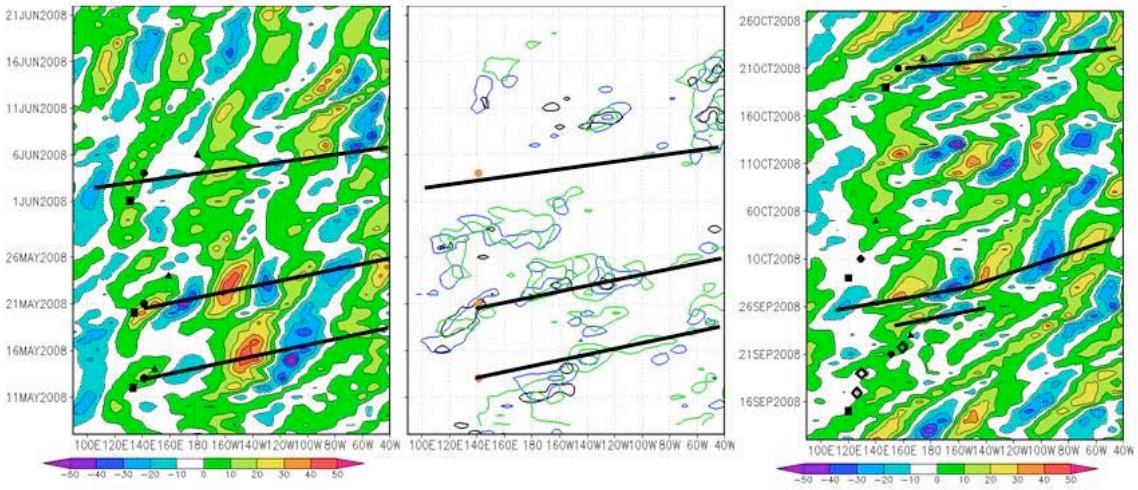

Figure 14. Hovmoeller plots across western North Pacific of a) 200 hPa meridional wind from 6 May – 22 June 2008 averaged from 40-60 N, b) 500 hPa standard deviation from ECMWF EPS for 3 day forecast (black), 5 day forecast (blue) and 7 day forecast (green), c) as a) but from 12 September to 27 October. Typhoon recurvature is marked on a) ,c) by a black square, ET by a black circle and decay point by a black triangle. The red circles on b) mark the ET time. Typhoons marked are (from top to bottom) Rammasun, Halong and Nakri in a),b) and Sinlaku, Jangmi and Bavi in c). Figure courtesy of Julia Keller. Data taken from the ECMWF YOTC analyses and the TIGGE database.

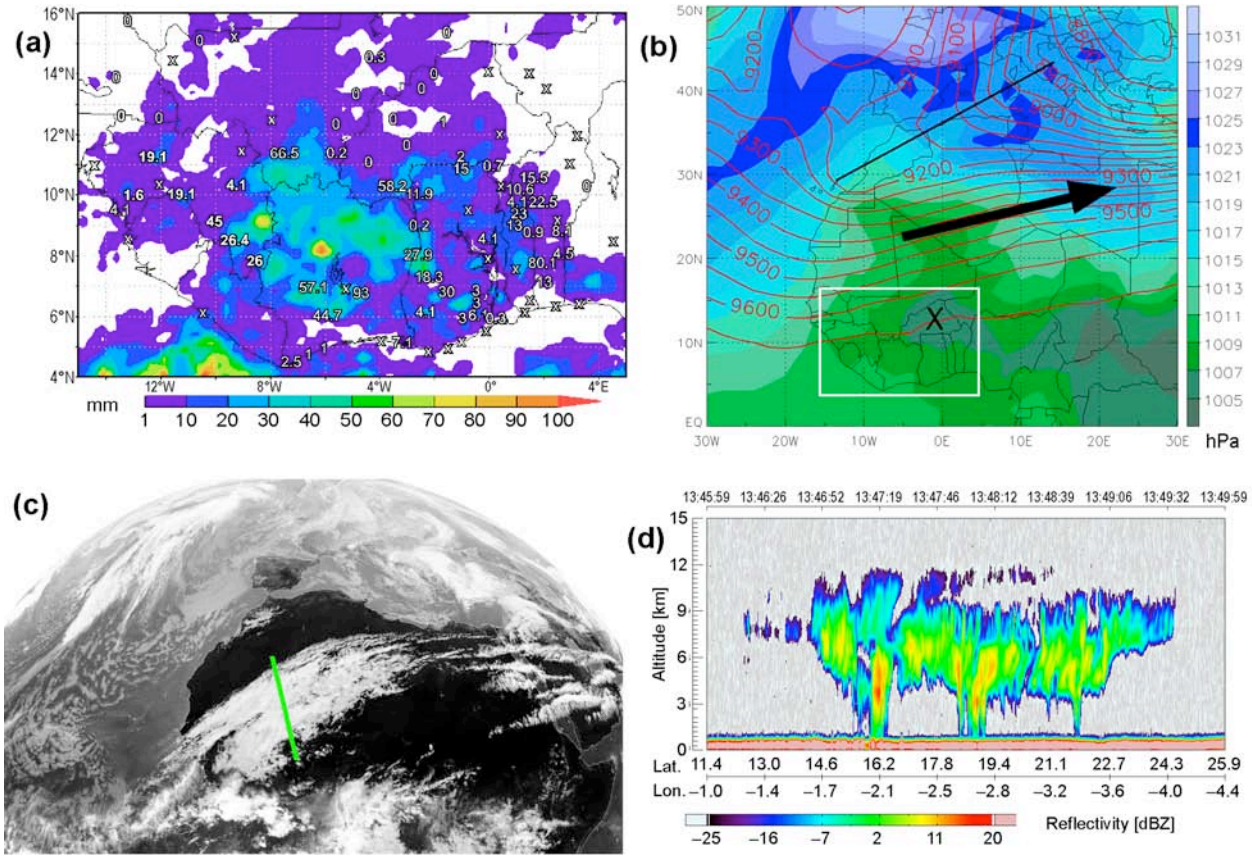

Figure 15. An unusual dry-season rainfall event in tropical West Africa during 16–20 February 2009. (a) Precipitation accumulated over the four-day period 0600 UTC 16 Feb. to 0600 UTC 20 Feb. 2009 from the TRMM 3B42 3-hourly rainfall product (colors) and from surface rain gauges (numbers). 'x' stands for 'no precipitation', '0' stands for 'traces of precipitation'. Some stations have gaps in their records and amounts must therefore be considered as lower bounds. (b) Geopotential height at 300 hPa (contours every 50 gpm) and mean seal-level pressure (colors) for 1200 UTC 16 Feb. 2009. Data are taken from the ECMWF YOTC analysis. The upper-troug axis, the subtropical jet streak, and the pressure minimum over Burkina Faso are indicated. The area shown in (a) is bordered by a white box. (c) Meteosat channel 9 (infrared; 10.8 μm) at 1200 UTC 19 Feb. 2009. (d) Vertical profile of reflectivity from the CloudSat Cloud Profiling Radar along the green line shown in panel (c) between 1346 and 1350 UTC 19 Feb. 2009.

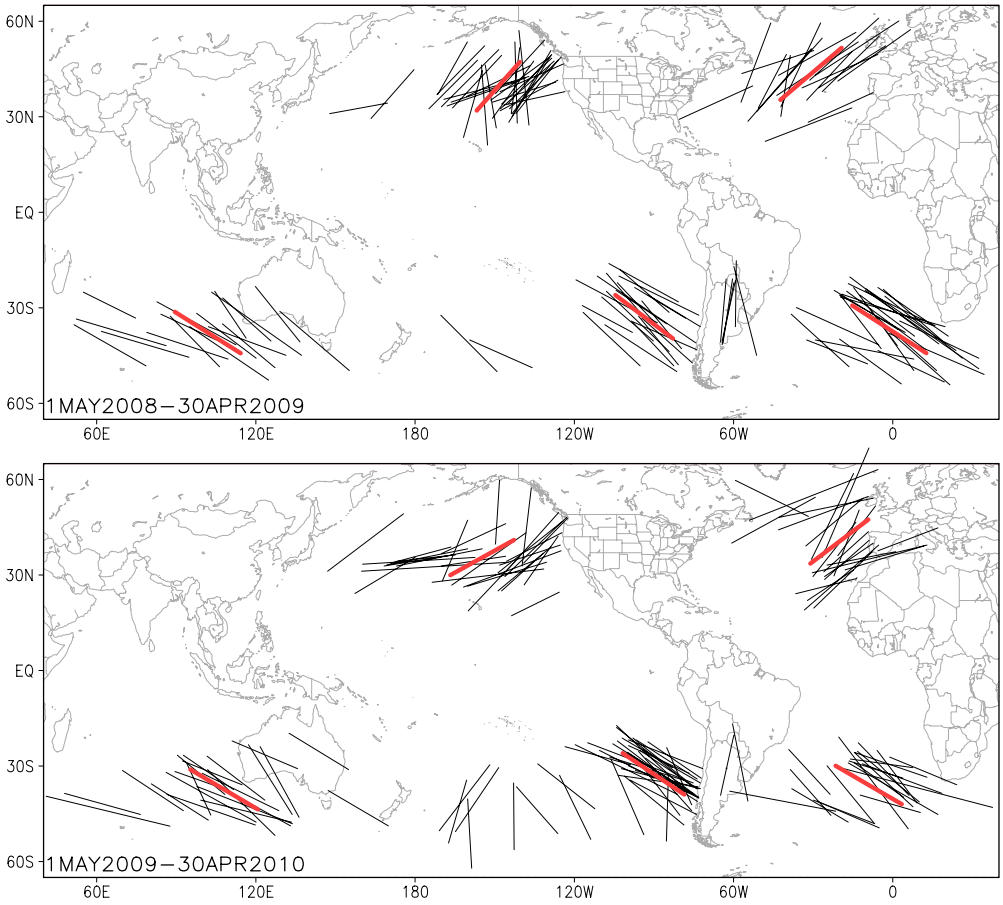

Figure 16. Approximate locations (main axes; black lines) of Atmospheric Rivers (ARs) during the YOTC period. Red lines indicate the mean locations of the ARs within each ocean basin. (The few isolated ARs west of 120°W were not included in the calculation for the southeastern Pacific.) ARs are identified as long (>2000 km), narrow (<1000km) plumes of enhanced (>2 cm) integrated water vapor (IWV) in the daily maps observed by the AIRS instrument, following the criteria set in Ralph et al. (2004). The AIRS version 5 level 3 standard retrievals are used, which are globally available on a 1°×1° grid. Daily means are first formed by weighting the ascending and descending satellite passes with the number of data counts within each grid cell. (**Upper**) 1 May 2008–30 April 2009. (**Lower**) 1 May 2009–30 April 2010.

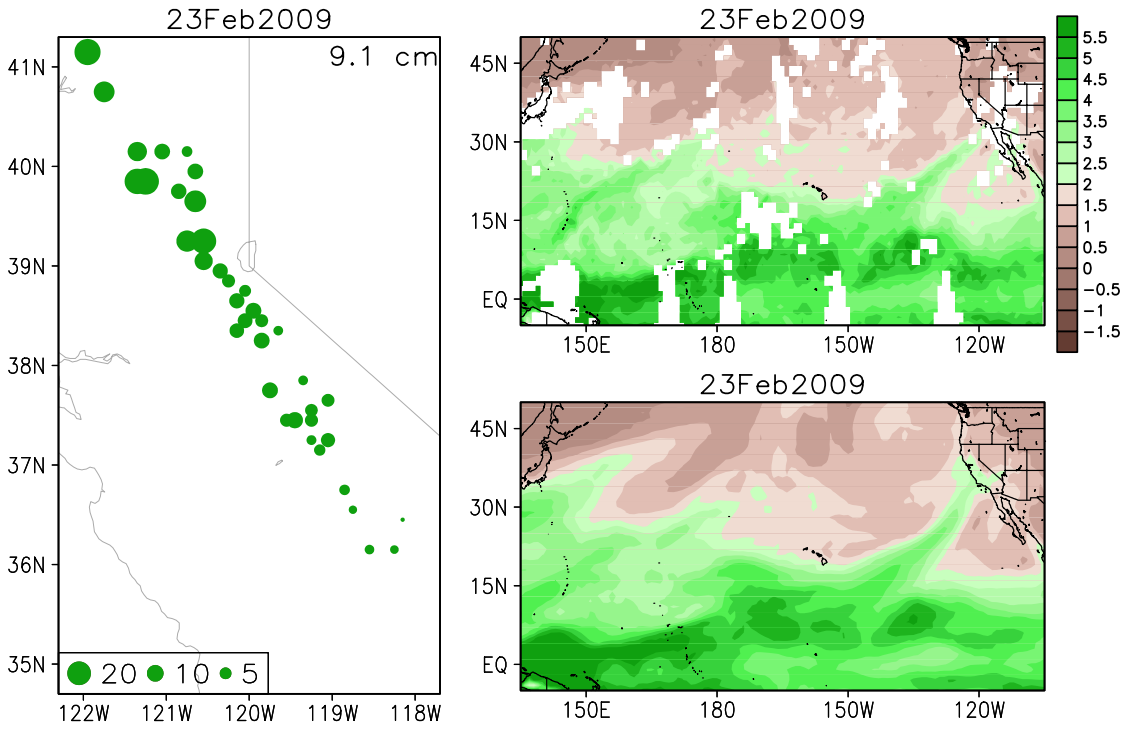

Figure 17. An atmospheric river (AR) event on 23 February 2009. (**Left**) Three-day cumulative precipitation (cm; centered on the AR date) observed at snow sensor sites across the Sierra Nevada. Data were obtained from the California Department of Water Resources (http://cdec.water.ca.gov/). Domain averaged precipitation is indicated in the upper right corner of the panel. (**Right**) Daily mean integrated water vapor (IWV) from (upper right) the AIRS instrument and (lower right) the ECMWF YOTC data set.

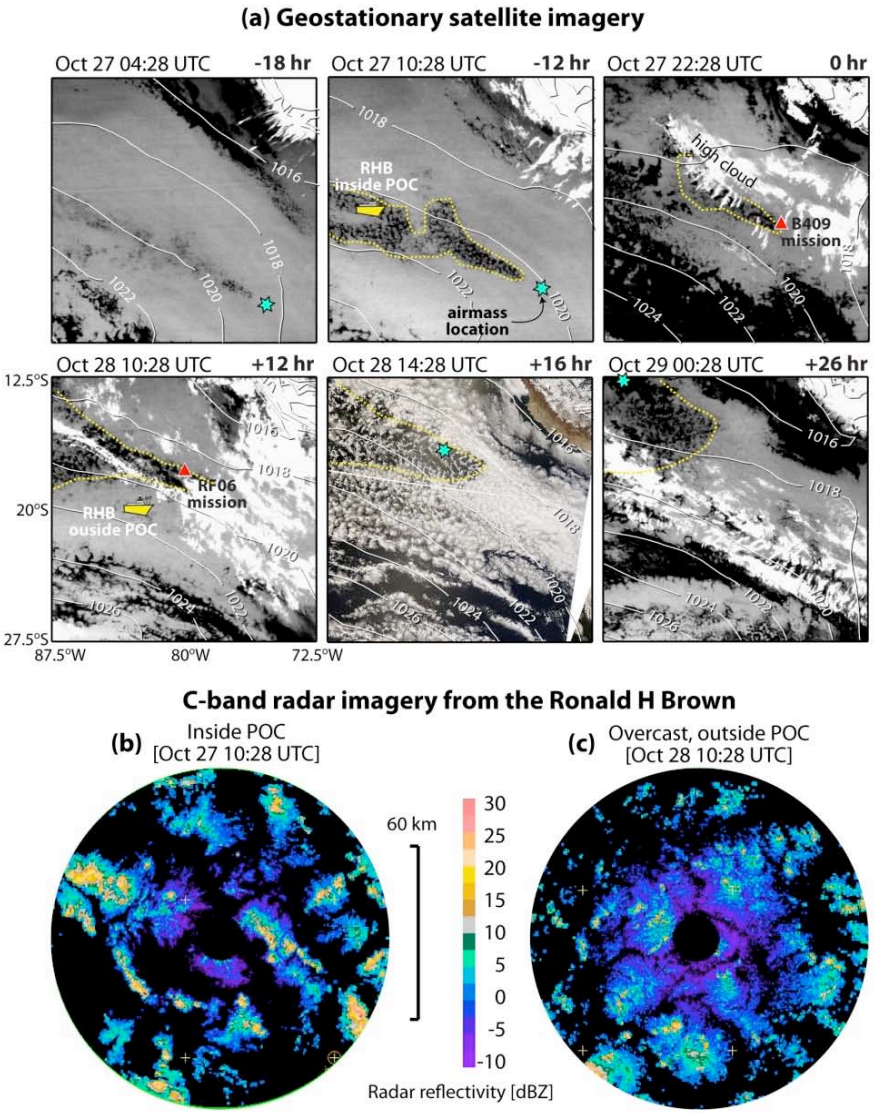

Figure SIDEBAR 1: (a) Thermal infrared and visible (Oct 28 14:28 UTC only) imagery for a 44 hour period encompassing the intensive measurement period in which a pocket of open cells (POC) is sampled by two aircraft (FAAM BAe-146 mission B409 and NSF/NCAR C-130 mission RF06) and the NOAA R/V Ronald H. Brown (RHB).The POC is delineated by the dashed yellow line. The blue star shows the location along a 925 hPa trajectory of an air parcel initiated at the location/time shown in the upper left panel. These locations are indicated by red triangles for the images when the aircraft were sampling. (b,c) Images of radar reflectivity from the C-band radar on the RHB for periods when the ship was inside the POC (b, see upper central satellite image for ship location) and outside the POC (c, see lower left satellite image for location of ship).